J Neurophysiol 123: 2101–2121, 2020.
First published April 22, 2020; doi:10.1152/jn.00706.2019.

RESEARCH ARTICLE | *Nervous System Pathophysiology*

Abnormal development of auditory responses in the inferior colliculus of a mouse model of Fragile X Syndrome

Anna O. Nguyen,[1] Devin K. Binder,[2,3] Iryna M. Ethell,[2,3] and Khaleel A. Razak[2,4]
[1]*Bioengineering Program, University of California, Riverside, California;* [2]*Graduate Neuroscience Program, University of California, Riverside, California;* [3]*Division of Biomedical Sciences, University of California, Riverside, California; and* [4]*Psychology Department, University of California, Riverside, California*

Submitted 14 November 2019; accepted in final form 22 April 2020

Nguyen AO, Binder DK, Ethell IM, Razak KA. Abnormal development of auditory responses in the inferior colliculus of a mouse model of Fragile X Syndrome. *J Neurophysiol* 123: 2101–2121, 2020. First published April 22, 2020; doi:10.1152/jn.00706.2019.—Sensory processing abnormalities are frequently associated with autism spectrum disorders, but the underlying mechanisms are unclear. Here we studied auditory processing in a mouse model of Fragile X Syndrome (FXS), a leading known genetic cause of autism and intellectual disability. Both humans with FXS and the *Fragile X mental retardation gene* (*Fmr1*) knockout (KO) mouse model show auditory hypersensitivity, with the latter showing a strong propensity for audiogenic seizures (AGS) early in development. Because midbrain abnormalities cause AGS, we investigated whether the inferior colliculus (IC) of the *Fmr1* KO mice shows abnormal auditory processing compared with wild-type (WT) controls at specific developmental time points. Using antibodies against neural activity marker c-Fos, we found increased density of c-Fos+ neurons in the IC, but not auditory cortex, of *Fmr1* KO mice at P21 and P34 following sound presentation. In vivo single-unit recordings showed that IC neurons of *Fmr1* KO mice are hyperresponsive to tone bursts and amplitude-modulated tones during development and show broader frequency tuning curves. There were no differences in rate-level responses or phase locking to amplitude-modulated tones in IC neurons between genotypes. Taken together, these data provide evidence for the development of auditory hyperresponsiveness in the IC of *Fmr1* KO mice. Although most human and mouse work in autism and sensory processing has centered on the forebrain, our new findings, along with recent work on the lower brainstem, suggest that abnormal subcortical responses may underlie auditory hypersensitivity in autism spectrum disorders.

NEW & NOTEWORTHY Autism spectrum disorders (ASD) are commonly associated with sensory sensitivity issues, but the underlying mechanisms are unclear. This study presents novel evidence for neural correlates of auditory hypersensitivity in the developing inferior colliculus (IC) in *Fmr1* knockout (KO) mouse, a mouse model of Fragile X Syndrome (FXS), a leading genetic cause of ASD. Responses begin to show genotype differences between postnatal days 14 and 21, suggesting an early developmental treatment window.

autism; development; Fragile X Syndrome; inferior colliculus; seizures; sensory hypersensitivity

INTRODUCTION

Fragile X Syndrome (FXS) is a leading genetic cause of intellectual disability and autism that affects ~1 in 4,000 males and 1 in 8,000 females. An expansion of CGG repeats in the 5′ untranslated region of the *Fragile X mental retardation 1* (*Fmr1*) *gene* causes its silencing and a loss of Fragile X Mental Retardation Protein (FMRP). FMRP is an RNA binding protein involved in translation regulation. The resulting abnormal protein synthesis in the brain during development leads to symptoms of FXS that include cognitive, anxiety and social deficits, hyperactivity, language impairments, increased susceptibility to seizures, and sensory impairments (Smith et al. 2012). A consistent and debilitating symptom of FXS is abnormal sensory reactivity (Rais et al. 2018), particularly hypersensitivity to sensory stimuli (Hitoglou et al. 2010; Rogers et al. 2003). Hypersensitivity manifests strongly in the auditory domain, but the underlying mechanisms are only beginning to be elucidated (Ethridge et al. 2016; Garcia-Pino et al. 2017; Wang et al. 2017).

An animal model of FXS, the *Fmr1* knockout (KO) mouse, displays several core FXS-like phenotypes including hyperactivity, social abnormalities, electrophysiological, and dendritic spine deficits (Bakker and Oostra 2003; Kazdoba et al. 2014). Importantly, the *Fmr1* KO mouse also shows auditory hypersensitivity, including enhanced cortical responses to sounds, increased propensity for AGS, and abnormal sensorimotor gating (Chen and Toth 2001; Frankland et al. 2004; Kokash et al. 2019; Rotschafer and Razak 2013; Wen et al. 2018). Electroencephalographic (EEG) recordings demonstrate remarkably similar phenotypes in the *Fmr1* KO mouse and humans with FXS (Castrén et al. 2003; Ethridge et al. 2017; Lovelace et al. 2016, 2018; Schneider et al. 2013). These include increased amplitude and reduced habituation of sound-evoked responses, increased resting gamma power, and reduced consistency in phase locking to amplitude-modulated sounds. In vivo single unit and EEG recordings from the auditory cortex of *Fmr1* KO mice show abnormally increased responses to sounds during development and in adults (Kulinich et al. 2020; Rotschafer and Razak 2013; Wen et al. 2018, 2019).

FMRP is expressed at multiple levels of the auditory system, and deficits in auditory processing are reported in the lower brainstem of the *Fmr1* KO mice (Beebe et al. 2014; Garcia-

Correspondence: K. A. Razak (Khaleel@ucr.edu).

Pino et al. 2017; Rotschafer and Cramer 2017; Rotschafer et al. 2015; Wang et al. 2014). A recent study showed that selective deletion of *Fmr1* from forebrain excitatory neurons only partially recapitulates cortical EEG phenotypes and showed that increased resting state low (30–60 Hz)- but not high (70–100 Hz)-gamma power reported in global *Fmr1* KO is present in the forebrain-specific knockout (Lovelace et al. 2020). These studies suggest that at least some of the abnormal responses recorded in the cortex are generated subcortically.

Audiogenic seizure (AGS) is a robust and consistently reported phenotype in the *Fmr1* KO mice, particularly between postnatal day (P)20 and P30 (Dölen et al. 2007; Michalon et al. 2012; Musumeci et al. 2007; Pacey et al. 2009; Yan et al. 2005). Multiple studies have suggested that abnormalities of the midbrain inferior and superior colliculi (IC, SC) underlie specific patterns of sensitivity and behaviors associated with AGS (Faingold and Randall, 1999; Faingold 2002; Millan et al. 1986). Indeed, Gonzalez et al. (2019) showed that AGSs are induced by *Fmr1* deletion in VGlut2-expressing excitatory neurons in the inferior colliculus (IC). We recently found elevated levels of matrix metalloproteinase-9 in the developing IC of *Fmr1* KO mice compared with wild-type (WT) mice and deficits in prepulse inhibition of acoustic startle in *Fmr1* KO mice (Kokash et al. 2019), further suggesting early developmental deficits in IC. These studies suggest that responses IC neurons of *Fmr1* KO mice are abnormal during development and may underlie auditory hypersensitivity. The main goal of this study was to test this hypothesis and to identify developmental changes in IC responses to sound in *Fmr1* KO mice.

We used two different methods to quantify IC auditory responses in WT and *Fmr1* KO mice. The first aim was to use immunostaining for c-Fos to determine the number of activated cells in the IC, auditory thalamus, and auditory cortex at P21 and P34. We found a significantly higher number of activated cells in the IC of the *Fmr1* KO compared with WT mice. Second, we performed in vivo single unit recordings from IC at P14, P21, and P34 to determine minimum thresholds, response magnitudes, frequency tuning, and responses to amplitude-modulated tones. We report significant genotype differences of IC responses that correlate with the development of auditory hyperresponsiveness in *Fmr1* KO mice.

METHODS

Animals. All animal procedures were approved by the University of California, Riverside Institution Animal Care and Use Committee. Breeding pairs of FVB.129P2-Fmr1tm1Cgr*/J* (*Fmr1* KO) and their congenic controls (WT) mice were obtained from Jackson Laboratories and bred in-house. All mice were housed in a 12:12-h light-dark cycle and given standard laboratory chow and water ad libitum. Immunostaining against c-Fos was done on the brain slices of P21–22 WT ($n = 16$), P34–39 WT ($n = 23$), P21–22 *Fmr1* KO ($n = 15$), and P34–39 *Fmr1* KO ($n = 23$) mice. Single-unit electrophysiological recordings were obtained from the IC of P14–15 WT ($n = 9$), P21–22 WT ($n = 11$), P34–39 WT ($n = 12$), P14–15 *Fmr1* KO ($n = 10$), P21–22 *Fmr1* KO ($n = 10$), and P34–39 *Fmr1* KO ($n = 9$) mice. These groups will be referred to as P14, P21, and P34 mice below. Male mice were used for all experiments.

Sound exposure paradigm. Our goal was to examine the levels of neural activity marker c-Fos in the auditory pathway of *Fmr1* KO mice in response to relatively loud sounds but without any overt motor behaviors associated with AGS. AGS behaviors include wild running and jumping and tonic seizure episodes that may lead to death (Dansie et al. 2013; Gonzalez et al. 2019). *Fmr1* KO mice, but not WT mice, are prone to AGS. Therefore, if the sound causes seizures, the associated motor responses involved would only be present in the KO mice and render the two groups incomparable in terms of sensory responses. Therefore, we performed pilot tests to identify the highest sound level that does not cause any motor responses associated with AGSs. These pilot data showed that the AGS threshold for P34 *Fmr1* KO mice was >90 dB SPL so we used 80 or 90 dB for 15 min (5- to 50-kHz bandwidth, 500-ms upward modulated frequency sweep followed by 500-ms downward modulated frequency sweep). However, 90-dB sounds induced AGSs in the P21 group, so we used 85 dB SPL in this age group with 1,000 ms of quiet in between each 1,000 ms of sound. Based on offline video analysis, none of the mice used showed any motor behaviors associated with AGSs. Therefore, there was no exclusion of mice to account for motor behaviors. To perform c-Fos immunostaining, up to four male mice in the P21 or P34 group were placed in a standard mouse cage with no food or water. Mice used for immunohistochemistry of c-Fos were habituated for 3 h in a sound attenuated booth (Gretch-Ken, Inc.) before stimulus presentation. This would facilitate isolation of c-Fos expression to the stimulus and minimize background c-Fos expression. In addition, these mice remained in the sound attenuation booth for 45 min after offset of the sound stimulus and before transcardial perfusion. Control groups underwent the same procedure except no sounds were presented. Auditory stimuli were generated using custom software (BATLAB, Dr. Don Gans, Kent State University or Sparkle, Portfors Laboratory, Washington State University) and delivered through a programmable attenuator (PA5, TDT) and a speaker (FT17H, Fostex International) placed face down on top of the cage lid. Sound levels were measured with a sound level meter (735, B&K Precision) at a distance from the speaker to the cage bottom. A lamp was used to provide light for a video camera to record behaviors during 5 min of baseline with no sound presentation and 15 min of sound presentation.

Immunohistochemistry. We examined the IC, the auditory thalamus, and core auditory cortex to determine if there are regional differences in c-Fos expression across genotypes. Two age groups of mice were used for the analysis of c-Fos+ cell density: P21 and P34. Mice were euthanized with sodium pentobarbital (Fatal-Plus, 125 mg/kg ip) for perfusion. Transcardial perfusion was done with cold 0.1 M PBS (pH 7.4) followed by cold 4% PFA (pH 7.6). The brain tissues were extracted and postfixed overnight in 4% PFA before storage in 0.1 M PBS at 4°C until further tissue processing in the future. The brains were cryoprotected in 30% sucrose for 2 days before being sectioned (CM 1860, Leica Biosystems) in the coronal plane at 40-μm thickness. All immunohistochemistry steps were done on a shaker at room temperature unless otherwise noted. For each mouse, two slices for each region of interest (IC, medial geniculate body, and auditory cortex) were used for c-Fos immunohistochemistry. Slices were chosen at ~50% in the rostrocaudal extent of the IC and MGB based on the Allen mouse brain atlas. This allowed for consistency in slice locations across mice. The shape of these nuclei also varies across the rostrocaudal extent, facilitating selection of comparable sections across mice. Consistency across mice in selecting the auditory cortex sections was based on the location of the dentate gyrus of the hippocampus. We have previously validated this method in Martin del Campo et al. (2012). Slices were washed three times for 5 min in 0.1 M PBS followed by blocking with 5% normal goat serum (NGS) for 1 h. Slices were then washed with PBS for 10 min followed by 0.5% triton X-100 for 10 min. Next, the slices were incubated overnight in 4°C in primary rabbit anti-c-Fos antibody [1:100; SC-52, Santa Cruz, Research Resource Identifier (RRID):AB_2106783[in 1% NGS and 0.1% Tween-20 in 0.1 M PBS. This antibody is commonly used in mouse studies (e.g., Howorth et al. 2009; Numa et al. 2019), including in studies of the central auditory system (Fulop et al. 2019). On the next day, the slices were washed three times for 5 min with PBS and incubated in secondary antibody (1:500; donkey anti-rabbit Alexa 594) with 1% NGS and 0.1% Tween 20 in PBS for

2 h. Then, the slices were washed in PBS three times for 5 min and mounted on a glass slide with a mounting medium (Vectashield H-1200, Vector Laboratories) and the edges were sealed (Cytoseal 60, Richard-Allan Scientific). The slides were stored in the dark at 4°C until imaging was done. Stained sections were imaged using a confocal microscope (SP5, Leica Microsystems) with ×10 objective and a stack of 20 optical images was collected with 1,024 × 1,024 resolutions at 2-μm z-steps. Image analysis was performed using ImageJ Software (NIH). Because the MGB is composed of multiple divisions with different functions, we evaluated c-Fos-positive cell density in each division separately using Allen Brain Atlas. The dimensions of the windows used for the cell counting in the different divisions of the MGB are provided in Table 1. The sizes of these windows were selected based on sufficient coverage of the divisions of interest across all photomicrographs. A 400-μm wide window that was at 45° angle to the midline of a coronal section was used as the counting window for the IC (Fig. 1, *A* and *B*). Large images were stitched as needed using the "stitch" plugin (Preibisch et al. 2009) for ImageJ to obtain high resolution images for counting. A rolling ball background subtraction was done for all images (rolling ball radius = 6.6 μm) facilitating a removal of smooth continuous backgrounds. c-Fos+ cell counts were based on intensity autothresholding of the pixels (Geometric Triangle Function) and size (>13.2 μm^2) in ImageJ for all images. The Geometric Triangle Function is an autothresholding feature of ImageJ. This allows consistent thresholding parameters to be applied to all images, thus ensuring uniform thresholding across slices. The triangle algorithm draws a line "b" from the maximum peak to the lowest value in an image's histogram. An orthogonal line "d" is computed from line "b" to the maximal distance of the histogram. A bin is formed from line 'd' to the maximum pixel intensity value. Then, all pixels in the image are converted to binary values (pixels within the bin as determined by the triangle algorithm and pixels not within the bin). Clusters of pixels that is >20 px^2 (13.2 μm^2) are counted as c-Fos+ cells.

In vivo electrophysiology recordings from IC. In vivo extracellular single unit recordings were conducted in urethane (1 g/kg)- and xylazine (20 mg/kg) (intraperitoenal injection)-anesthetized mice. Supplemental doses of anesthesia were given during recording sessions, as needed. A craniotomy was performed using a micro drill (Foredom Electric Co.) with coordinates based on skull landmarks. The IC was identified based on the transverse sinus vein, auditory responses, tonotopy, and post hoc histology from Fluoro-Ruby dye injected in the recording site. A negative feedback rectal thermometer was used to maintain the temperature of the mice at 38 ±1°C throughout the recording session. A calibrated speaker was placed contralateral to the recorded IC at a 45° angle and 6 cm away from the ear. A glass electrode (1 M NaCl, 2-10 MΩ impedance) was advanced using a micromanipulator (Kopf 2660) to depths between 200-2000 μm in the IC. Sound stimulation and data acquisition were driven by SPARKLE software (Sparkle Data Acquisition, Portfors Lab). Single units were isolated and identified based on amplitude and constancy of spikes. Unless otherwise noted, each stimulus was repeated 20 times with a 2-Hz repetition rate. The stimulus duration was 50 ms including a 2-ms rise/fall time. The recording window used was 250 ms from stimulus onset except for the sinusoidal amplitude modulated (SAM) tones, in which the recording window was 1,000 ms. Poststimulus time histogram data were analyzed offline. The number of neurons recorded from each group were as follows: n = 78 from P14-15 WT, n = 77 from P21-22 WT and n = 102 from P34-39 WT; n = 81 from P14-15 *Fmr1* KO, n = 84 from P21-22 *Fmr1* KO, and n = 83 from P34-39 *Fmr1* KO mice. Upon isolation of a neuron, spontaneous activity and response selectivity were quantified as described below.

Table 1. *Window sizes for c-Fos+ cell analysis in the MGB subdivisions*

Medial Geniculate Body (MGB) Subnuclei	Cell Count Window Size, μm
Suprageniculate nucleus (SGN)	100 × 175
Dorsal division of the MGB (MGd)	250 × 200
Ventral division of the MGB (MGv)	250 × 350
Medial division of the MGB (MGm)	200 × 250
Peripeduncular nucleus (PP)	530 × 200

Spontaneous activity and frequency response area. Spontaneous activity was recorded within the 250-ms recording window in the absence of any stimuli. The number of action potentials in the recording window was sampled over 20 repetitions (with no sound, 2-Hz repetition rate). Frequency tuning curves were constructed by measuring responses to tones with frequencies between 4 and 48 kHz in 4-kHz steps, and sound levels between 10- and 90-dB SPL in 10-dB steps. Each frequency/sound level combination was presented 20 times with a 2-Hz repetition rate. Characteristic frequency (CF) was defined as the frequency to which the neuron responded at the lowest sound level tested. Bandwidth (BW)10, BW20, and BW30 was the range of frequencies to which the neuron responded at 10 dB, 20 dB, and 30 dB above minimum threshold, respectively.

Rate-level functions. We determined the rate-level function of each neuron to quantify the changes in response magnitude with increasing sound levels. The CF tone was presented at levels between 10- and 90-dB SPL in a pseudorandom manner. The number of action potentials over 20 repetitions of each sound level was counted to plot the rate-level function. Percent turnover (%TO) and dynamic range were calculated from the rate-level functions as defined by (Phillips and Kelly 1989). %TO was taken as $\%TO = \frac{\text{Max Response} - \text{Response to 90 dB SPL}}{\text{Max Response}} \times 100$. The higher the value of %TO, the more nonmonotonic is the relationship between sound level and response magnitude and indicates that the response increases and then decreases as sound levels increase. A low %TO indicates either that the response increases continuously with sound level or that it saturates. We hypothesized that the *Fmr1* KO IC neurons would show reduced %TO compared with WT IC neurons. The dynamic range is the range of sound levels over which the response increases from 10% to 90% of maximum response. Across the population, the dynamic range is indicative of how rapidly the IC gets activated with increasing sound levels. We hypothesized that the *Fmr1* KO IC neurons would show narrower dynamic range compared with WT IC neurons.

Response magnitude and first spike latency. The average number of spikes per stimulus and the median first spike latency was calculated from the response of neurons to 20 repetitions (2-Hz rate) of CF tones presented at 15 dB and 30 dB above minimum threshold.

Selectivity for sinusoidal amplitude modulated sounds. Sinusoidal amplitude modulated (SAM) tones were used to determine temporal properties of IC neurons. The carrier frequency was at CF presented 15 dB above minimum threshold (500-ms duration and 2-ms rise/fall time). The recording window was 1,000 ms in duration. The carrier tone was 100% depth modulated at the following frequencies: 5, 10, 20, 50, 100, and 200 Hz. Rate modulation transfer function (rMTF) was defined as the number of spikes per stimulus presentation for the duration of the stimulus presentation (500 ms). Temporal modulation transfer function (tMTF) was quantified as the vector strength (VS; Goldberg and Brown 1969). Each spike time was correlated to the period phase (0–360°). The VS was determined at each modulation frequency (5, 10, 20, 50, 100, and 200 Hz). In the tMTF period analysis, the first 100 ms of the recording duration was not included to omit the onset response to the sound stimulus.

Statistical analysis. For the c-Fos analysis, the average of cell counts from two slices per brain region per animal was used with animal number as sample size. Mice were separated into quiet and sound-exposed groups. The P21 mice received one sound level (85 dB), and the P34 groups received one of two sound levels (80 or 90

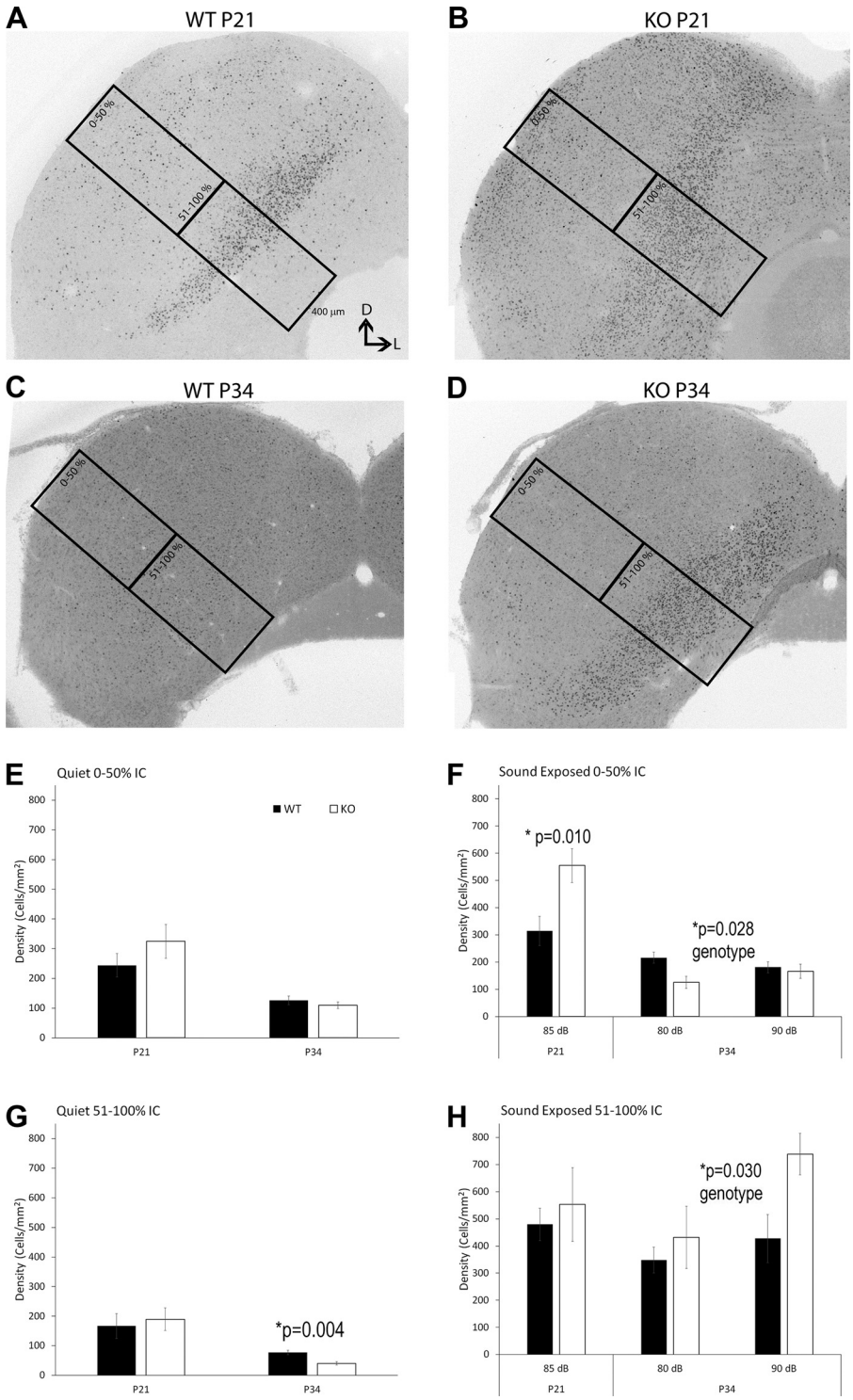

Fig. 1. c-Fos+ cell density is increased in the inferior colliculus (IC) of *Fmr1* knockout (KO) mice. *A* and *B*: example photomicrographs of c-Fos immunoreactivity in the IC obtained from postnatal day (P)21 wild-type (WT) (*A*) and P21 *Fmr1* KO mice (*B*) following sound exposure (85 dB). *C* and *D*: example photomicrographs of c-Fos immunoreactivity in the IC at P34 following 90 dB sound exposure of WT (*C*) and *Fmr1* KO mice (*D*). Rectangular boxes in *A–D* show counting windows (400-μm width) that span the IC in a dorsolateral to medioventral direction. *E*: for the 0–50% counting window (dorsolateral half), there were no significant genotype differences in the density of c-Fos+ cells at both ages in the quiet group. *F*: in the sound-exposed group, for the 0–50% window, there was a significant increase in c-Fos+ cell density at P21 in *Fmr1* KO mice ($*P = 0.010$) and a genotype effect at P34 ($P = 0.028$). *G*: in the 51–100% window (medioventral half), there was a significant decrease in c-Fos+ cell density in the *Fmr1* KO mice at P34 under the quiet condition ($*P = 0.004$). *H*: for the sound-exposed group, there was no genotype difference at P21 in 51–100% window of the IC. At P34, there was significant increase in c-Fos+ cell density in *Fmr1* KO compared with WT ($P = 0.030$) mice. Error bars show SE.

dB). If the counts of c-Fos+ cells within a brain region showed normal distribution, then a Student's *t* test was used for genotype comparisons. If any data set within a brain region was not normally distributed, then all genotype comparisons within that brain region used the nonparametric Mann-Whitney *U* test. Genotype differences were analyzed by comparing the means of *Fmr1* KO versus WT separately for P21 and P34 groups. For the electrophysiology data, a two-way ANOVA with age and genotype as factors was performed to test main effects and interactions. The number of neurons was used as sample size for electrophysiology data. Unless otherwise noted, $P < 0.05$ was considered significant for ANOVA, Student's *t* test, and Mann-Whitney *U* test.

RESULTS

Density of c-Fos+ cells was higher in the IC of Fmr1 KO compared with WT mice at P21 and P34. The first major aim of the study was to determine potential genotype- and age-dependent differences in the number of c-Fos+-activated cells

in the IC, MGB, and auditory cortex. The density of c-Fos+ cells was counted in the quiet and sound-exposed conditions in P21 and P34 mice of both genotypes, corresponding to high and low AGS susceptible ages, respectively (Musumeci et al. 2000). After habituation for 3 h in a sound-attenuated booth, a siren-like sound (alternating 5- to 50-kHz upsweep for 500 ms and 50- to 5-kHz downsweep for 500 ms) was played for 15 min. Following perfusion, images of c-Fos-immunoreactive labeling were collected and a 400-μm-wide window, drawn diagonally in the dorsolateral to ventromedial direction of the IC, was selected for cell counting (Fig. 1, *A–D*). This window was further subdivided into two halves for analysis covering 0–50% and 51–100% of the IC in the dorsolateral to ventromedial direction.

In the quiet condition, a Student's *t* test showed no significant genotype difference in the 0–50% region of the IC at P21 [$t(11) = -1.186$, $P = 0.261$] or P34 [Fig. 1*E*; $t(12) = 0.841$, $P = 0.417$]. In the 51–100% region (Fig. 1*G*), there was also no significant genotype difference at P21. However, at P34 the density of c-Fos+ cells was significantly lower in the 51–100% region of the IC *Fmr1* KO mice compared with WT mice [$t(12) = 3.618$, $P = 0.004$]. Thus, for ambient sound levels, the density of c-Fos+ cells in the IC was not higher in the *Fmr1* KO mice compared with WT mice at either P21 or P34.

However, when sounds were presented, the *Fmr1* KO mouse IC showed higher c-Fos+ cell density than WT group at both P21 and P34. Only a single sound level (85 dB) was tested for the P21 group so the data were analyzed using a Student's *t* test. At P34, we tested mice at either 80- or 90-dB SPL and used a two-way ANOVA (sound level and genotype as factors) for the c-Fos+ cell density analysis. At P21, there was a significant increase in the sound-evoked c-Fos+ cell density in the 0–50% IC window of *Fmr1* KO mice compared with WT mice [Fig. 1*F*, $t(16) = -2.907$, $P = 0.010$]. Interestingly, for the P34 group, there was a significant decrease in the density of c-Fos+ cells in the 0–50% IC window of *Fmr1* KO mice compared with the WT mice [$F(1,27) = 5.415$, $P = 0.028$].

In the more ventromedial (51–100%) half of the IC (Fig. 1*H*), there was no significant difference at P21 between WT and *Fmr1* KO mice [$t(16) = -1.444$, $P = 0.168$]. At P34, c-Fos+ cell density was significantly higher in *Fmr1* KO mice compared with WT mice [$F(1,27) = 5.216$, $P = 0.030$]. There was also a main effect of sound level with significantly higher c-Fos+ cell density at 90 dB compared with an 80-dB sound level [$F(1,27) = 4.998$, $P = 0.034$]. There was no genotype × sound interaction [$F(1,27) = 1.734$, $P = 0.199$] at P34. Thus, when exposed to sound, c-Fos+ cell density was higher in the IC of the *Fmr1* KO than WT mice, suggesting auditory hyperresponsiveness in the IC at both P21 and P34. The region of the IC showing increased c-Fos+ cell density in the *Fmr1* KO mice shifts with age (P21→P34) from more dorsolateral IC to more ventromedial locations.

Division-specific genotype differences in c-Fos+ cell density in the medial geniculate body. The MGB comprises multiple divisions, including the medial (MGm), the ventral (MGv), the dorsal (MGd) divisions, and the suprageniculate nucleus (SGN) (Fig. 2). The adjacent peripeduncular nucleus (PP) may also be involved in auditory processing through reciprocal connections with the IC (Arnault and Roger 1987). For the quiet condition data, a Mann-Whitney *U* test was used for genotype comparison in each MGB division. At P21, there was a significant increase in c-Fos+ cell density in *Fmr1* KO mice compared with WT mice in the MGm ($U = 5$, $P = 0.014$). There was no significant difference in other divisions of the MGB at P21 [PP ($U = 20$, $P = 0.604$), MGv ($U = 3.5$, $P = 0.543$), MGd ($U = 18$, $P = 0.420$), and SGN ($U = 14.5$, $P = 0.217$)]. At P34, there was a significant increase in c-Fos+ cell density in *Fmr1* KO, compared with WT, mice in the MGv ($U = 8$, $P = 0.01$) but not in the other divisions [PP ($U = 26$, $P = 0.574$), MGd ($U = 15.5$, $P = 0.083$), MGm ($U = 17$, $P = 0.106$), and SGN ($U = 28.5$, $P = 0.712$)].

In the sound-exposure condition, at P21, there was a significant increase in c-Fos+ cell density in the SGN ($U = 7.5$, $P = 0.003$) and PP ($U = 19$, $P = 0.05$) of the *Fmr1* KO mice compared with the WT. All other divisions showed no significant differences [MGv ($U = 38.5$, $P = 0.858$), MGd ($U = 22$, $P = 0.102$), and MGm ($U = 20$, $P = 0.069$)]. At P34, no genotype differences were present in any MGB division for sounds presented at 80 dB SPL: PP ($U = 17.5$, $P = 0.370$), MGv ($U = 17.5$, $P = 0.368$), MGd ($U = 13.5$, $P = 0.158$), MGm ($U = 24$, $P = 0.949$), and SGN ($U = 20$, $P = 0.565$). When sound was at 90 dB, only the PP ($U = 29$, $P = 0.05$) showed a genotype difference. There were no differences in the other divisions [MGv ($U = 33$, $P = 0.083$), MGd ($U = 43$, $P = 0.283$), MGm ($U = 30.5$, $P = 0.061$), and SGN ($U = 54$, $P = 0.760$)]. Thus, for ambient sound conditions, *Fmr1* KO mice show increased number of c-Fos+-activated cells in the MGm and MGv. When sound was presented, the SGN and PP showed higher number of c-Fos+ cells in *Fmr1* KO mice.

Auditory cortex does not show increased c-Fos+ cell density in Fmr1 KO mice. Single unit recordings from auditory cortex (Wen et al. 2018) showed higher response magnitude in P21 *Fmr1* KO mice compared with WT mice, suggesting hyperactivity of individual neurons in the auditory cortex. Here, to investigate whether more neurons were activated in the auditory cortex of *Fmr1* KO mice, we quantified the density of c-Fos+ cells (Fig. 3). A 400-μm-wide rectangular window that spanned the length of cortical layers I-VI was used to quantify c-Fos+ cell density (Fig. 3, *A* and *B*). In the quiet condition (Fig. 3*C*), there were no genotype differences in the number of c-Fos+ cells in the auditory cortex of WT and *Fmr1* KO mice at P21 ($U = 16$, $P = 0.302$) or P34 ($U = 26$, $P = 0.529$; Fig. 3*C*, *left*). In the sound exposure condition (Fig. 3*D*), there was no significant genotype difference in c-Fos+ cell density at P21 ($U = 25$, $P = 0.321$). At P34, Mann-Whitney tests showed a significant genotype difference when mice were exposed to 80 dB ($U = 6$, $P = 0.018$), but the number of c-Fos+ cells was lower in the *Fmr1* KO mouse cortex. There was no difference for the 90-dB sound level ($U = 33$, $P = 0.364$).

Electrophysiology. Extracellular single unit recordings were obtained from the IC in both genotypes at three different developmental ages: P14, P21, and P30. Spontaneous activity, rate-level functions, frequency tuning curves, and responses to amplitude-modulated tones were compared across age and genotype.

Spontaneous activity of IC neurons shows CF-specific genotype differences. Spontaneous activity was measured by counting the number of spikes over 20 repetitions of the recording window (250 ms) with no sound stimulus. The average spontaneous activity across all recorded neurons for each genotype and age was then used in a two-way ANOVA (age and genotype as factors) to identify statistical differences. The overall spontaneous activity in the IC was low, likely due

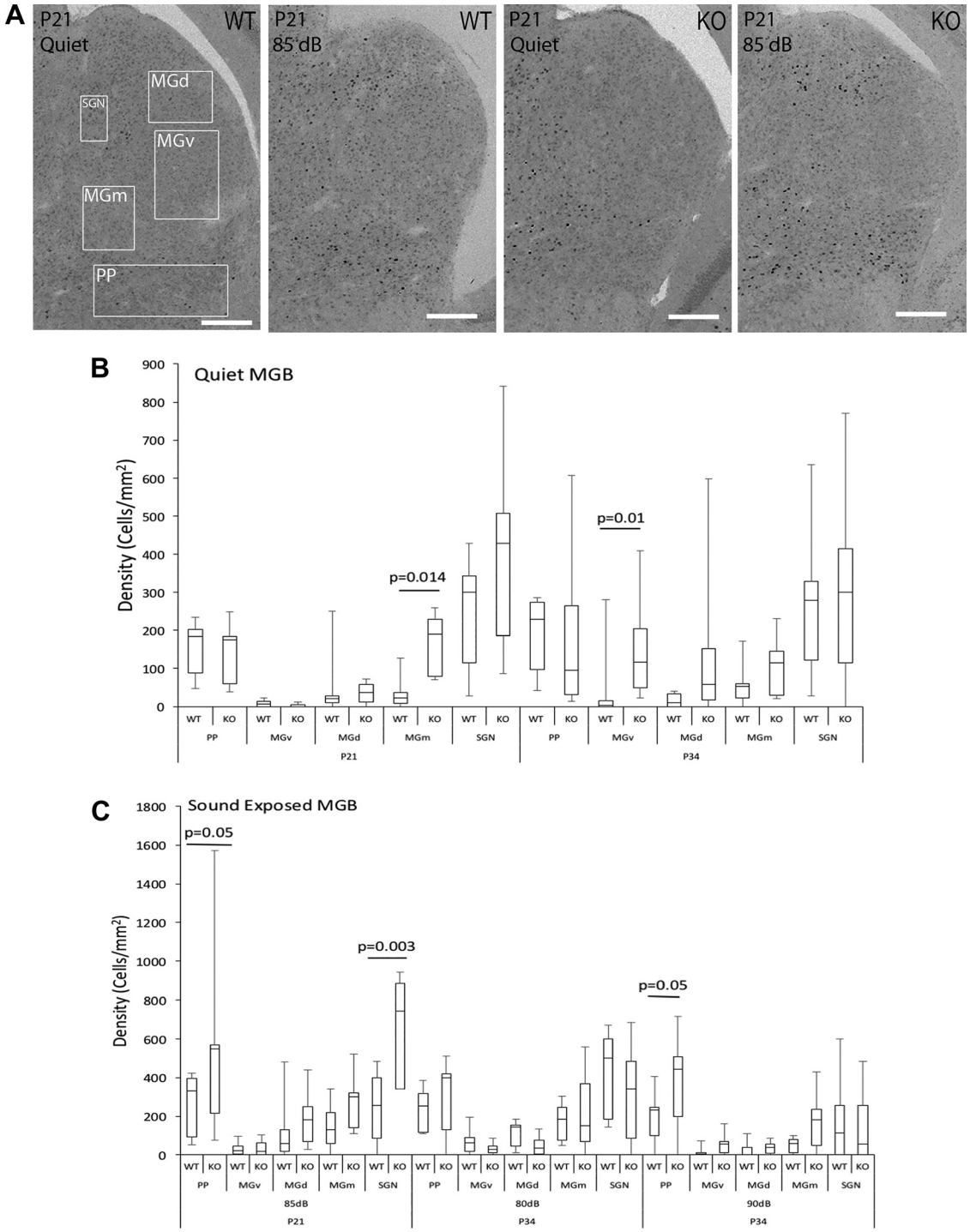

Fig. 2. Subdivision-specific genotype differences in c-Fos+ cell density in the medial geniculate body (MGB). *A*: example photomicrographs of c-Fos immunoreactivity in the MGB of wild-type (WT) and *Fmr1* knockout (KO) mice obtained at postnatal day (P)21. *B*: box and whisker plot of c-Fos+ cell density in the quiet groups at P21 and P34. *C*: box and whisker plot of c-Fos+ cell density in the sound-exposed groups at P21 and P34. Scale bar = 200 μm. SGN, suprageniculate nucleus; PP, peripeduncular nucleus; MGd, dorsal division of the MGB; MGv, ventral division of the MGB; MGm, medial division of the MGB.

to the anesthesia (Fig. 4*A*). However, it was possible to detect a significant main effect of age [$F(2,499) = 11.153$, $P = 0.000018$] with Bonferroni post hoc comparison showing a reduction in spontaneous activity with age (P14 vs. P21, $P = 0.024$; P14 vs. P34, $P = 0.000007$; and P21 vs. P34, $P = 0.124$). There was no main effect of genotype [$F(1, 499) = 2.333$, $P = 0.127$] or significant genotype × age interaction [$F(2,499) = 1.186$, $P = 0.306$]. Thus, when all the neurons were considered together, spontaneous activity decreased during development in the IC, with no genotype differences.

Because there were regional genotype differences in the c-Fos+ cell density in the IC, we analyzed the electrophysiology data by classifying neurons according to CF, with low and

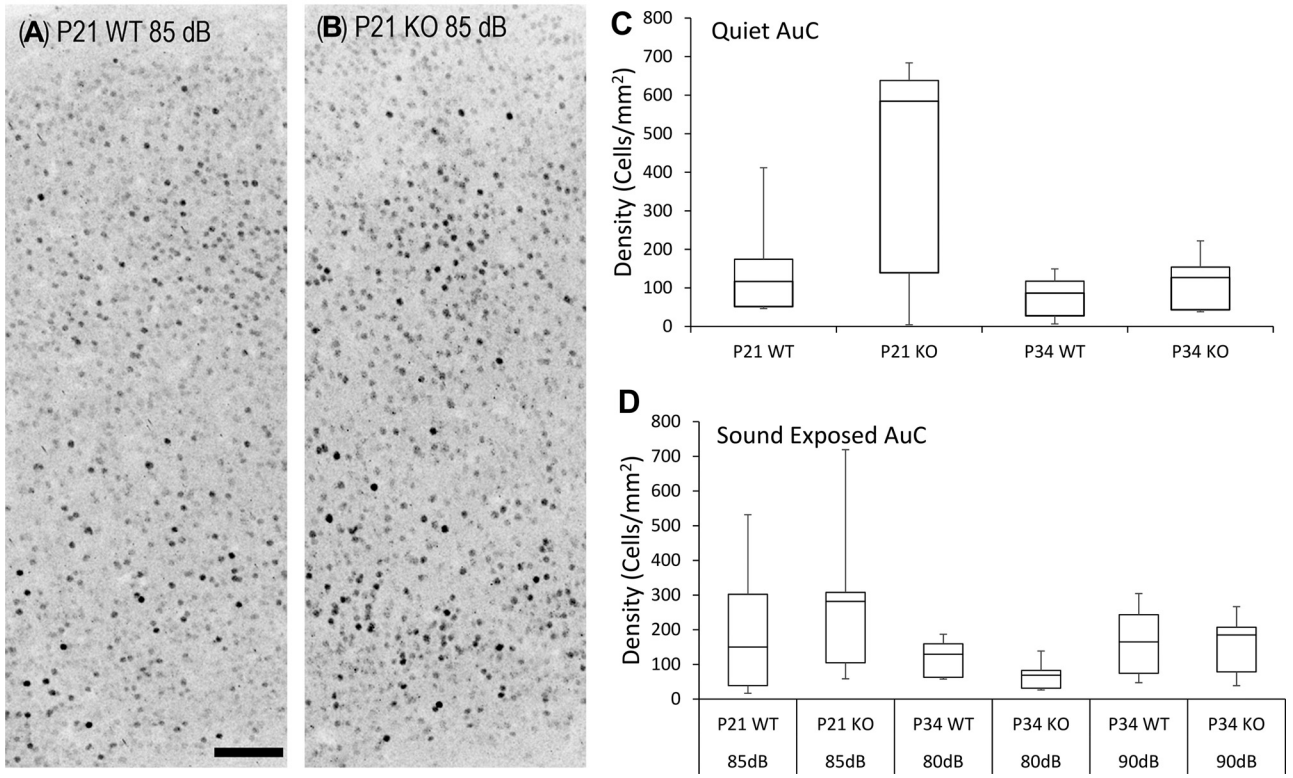

Fig. 3. Genotype comparisons of c-Fos+ cell density in the auditory cortex. *A* and *B*: example photomicrographs of sound driven c-Fos immunoreactivity in auditory cortex (AuC) of postnatal day (P)21 wild-type (WT; *A*) and *Fmr1* knockout (KO; *B*) mice. All 6 cortical layers are shown in *A* and *B* with a pial surface at *top*. Scale bar = 100 μm. *C*: box and whisker plot of c-Fos+ cell density in the quiet condition. *D*: box and whisker plot of c-Fos+ cell density in the sound-exposed condition.

high CF groups separated with a 20-kHz cut-off range. We chose the 20-kHz cut-off frequency because the IC tonotopic map splits approximately into two halves at this CF (Felix and Portfors 2007). The full statistics for the CF-classified data are provided in Table 2. *Fmr1* KO neurons with CF<20 kHz produced more spontaneous spikes than their WT counterparts. There was an interaction between age and genotype, but no main effect of age. For neurons with CF ≥20 kHz, we observed no main effect of genotype or significant genotype × age interaction. A significant main effect of age was present, with Bonferroni post hoc comparison showing a decrease in spontaneous activity with age (P14 vs. P21, $P = 0.000182$; P14 vs. P34, $P < 0.0001$; P21 vs. P34, $P = 0.015$) (Fig. 4*B*). In terms of spontaneous activity in the IC, these data indicate a larger effect of genotype in neurons with CF <20 kHz and an effect of age in neurons with CF ≥20 kHz.

Minimum thresholds of IC neurons show CF-specific genotype differences. We next compared minimum threshold (MT), defined as the lowest sound level that evoked a response to tones. When all neurons were considered regardless of CF, there was no significant main effect of genotype [$F(1,501) = 1.834$, $P = 0.176$] (Fig. 4*C*). Analysis demonstrated a significant genotype × age interaction [$F(2,501) = 3.818$, $P = 0.023$] and a main effect of age [$F(2,501) = 11.586$, $P = 0.000012$] with Bonferroni post hoc (P14 vs. P21, $P = 0.000115$; P14 vs. P34, $P = 1.00$; P21 vs. P34, $P = 0.000037$), showing the lowest average MT at P21 compared with P14 and P34.

When separated by CF (Table 2), neurons with CF <20 kHz showed no main effect of genotype or genotype × age interaction for MT. There was a significant main effect of age with Bonferroni post hoc analysis showing a difference in MT between P14 versus P21 ($P = 0.001$) and P21 versus P34 ($P < 0.0001$) but not for P14 versus P34 ($P = 0.261$) (Fig. 4*D*). For neurons with CF ≥20 kHz, a significant main effect of genotype was seen with a lower MT in *Fmr1* KO compared with WT IC. There was no genotype × age interaction. A main effect of age ($P < 0.0001$) was also observed for MT with Bonferroni post hoc comparison showing a difference between P14 versus P21 ($P = 0.000005$) and P14 versus P34 ($P = 0.007$) but not P21 versus P34 ($P = 0.105$) (Fig. 4*D*). These data suggest that reduced MT in high CF neurons may underlie auditory hyperresponsiveness in *Fmr1* KO mice.

IC neurons in Fmr1 KO mice are hyperresponsive to tones. Response magnitude to 20 repetitions of the CF tone was measured and compared across age and genotype. For all neurons combined (Fig. 5*A*), the average response magnitude at MT + 15 dB (15 dB above threshold) showed no significant genotype × age interaction [$F(2,481) = 1.495$, $P = 0.225$]. There was a significant main effect of genotype with more spikes/stimulus in *Fmr1* KO mice compared with WT mice [$F(1,481) = 5.249$, $P = 0.022$]. There was also a main effect of age [$F(2,481) = 6.257$, $P = 0.002$] with Bonferroni post hoc comparisons being significant for P21 versus P34 ($P = 0.004$) and P14 versus P34 ($P = 0.005$) but not for P14 versus P21 ($P = 1.00$) (Fig. 5*A*). Sound-evoked responses were reduced with age in both WT and KO IC. For CF tone responses at MT + 30 dB (Fig. 5*B*), there was a significant genotype × age interaction [$F(2,477) = 4.303$, $P = 0.014$)]and a significant main effect of genotype [$F(1,477) = 4.772$, $P = 0.029$], with *Fmr1* KO mouse neurons responding with more spikes than

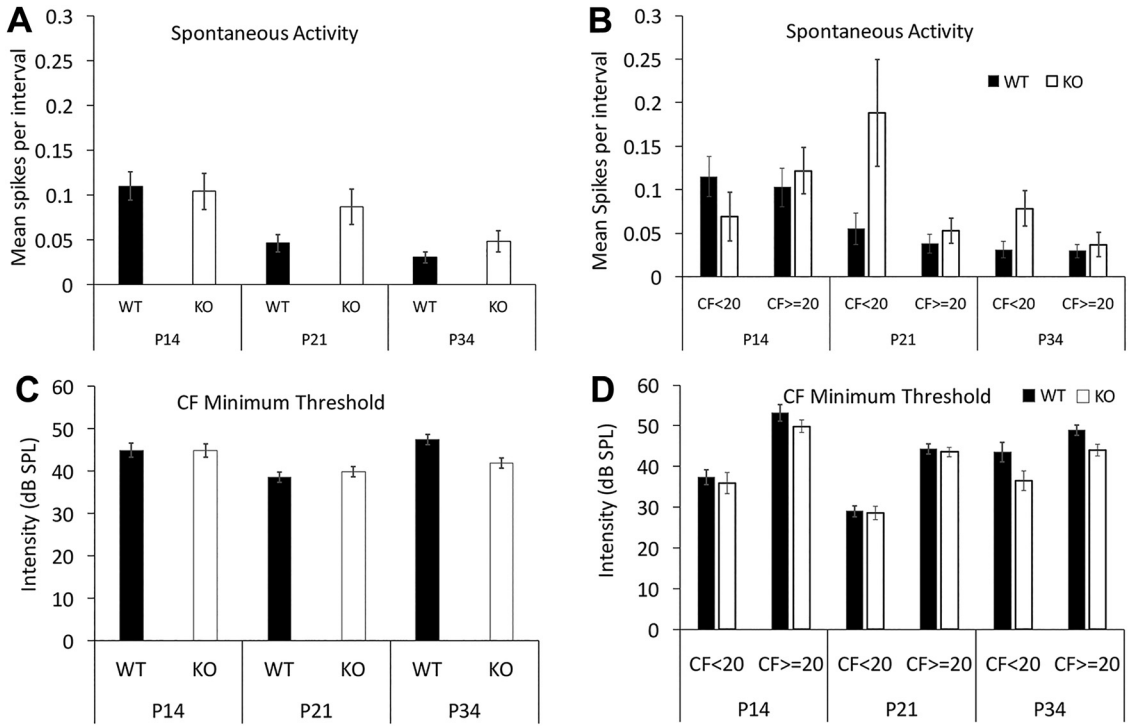

Fig. 4. Spontaneous activity and minimum threshold of *Fmr1* knockout (KO) and wild-type (WT) inferior colliculus (IC) neurons at postnatal day (P)14, P21, and P34. The graphs in *A* and *B* show the average number of spikes per acquisition window (250 ms, 20 repetitions) in the absence of any stimulus. *A*: two-way ANOVA (age × genotype) shows a main effect of age ($P = 0.000018$), with spontaneous firing rate decreasing across development. *B*: for neurons with characteristic frequency (CF) <20 kHz, a two-way ANOVA revealed significant interaction between genotype × age ($P = 0.008$) and significant main effects of genotype but no significant main effect of age (genotype: $P = 0.04$; age: $P = 0.08$). For neurons with CF ≥20 kHz, there was no significant genotype × age interaction or main effects of genotype ($P = 0.949$, $P = 0.335$, respectively). There was a significant main effect of age ($P = 0.000004$). *C*: the average minimum threshold at CF for neurons in IC showed no main effects of genotype ($P = 0.176$). There was a significant interaction between genotype × age and a main effect of age ($P = 0.023$, $P = 0.000012$, respectively). *D*: for neurons with CF <20 kHz, there was no significant genotype × age interaction or main effect of genotype ($P = 0.282$, $P = 0.09$, respectively). There was a significant main effect of age ($P = 0.000004$). For neurons with CF ≥20 kHz, there was no significant interaction between genotype × age ($P = 0.299$). There was a significant main effect for both genotype and age ($P = 0.000005$). Error bars show SE.

WT neurons. There was a significant main effect of age [$F(2,477) = 6.313$, $P = 0.002$] with Bonferroni post hoc tests revealing no significant differences in P14 versus P21 ($P = 1.00$) but a significant reduction with age in P21 versus P34 ($P = 0.001$) and P14 versus P34 ($P = 0.019$) comparisons.

For neurons with CF<20 kHz (Table 2), responses to tones at MT + 15 dB showed a significant main effect of genotype with *Fmr1* KO neurons responding more than WT neurons (Fig. 5*C*). There was no significant main effect of age or genotype × age interactions. Similarly, for tones presented at

Table 2. *Statistical analysis of data classified according to CF (<20 kHz vs. ≥20 kHz) for spontaneous activity, minimum threshold, and sound-driven activity at MT + 15 dB and MT + 30 dB*

	CF <20 kHz	CF> = 20 kHz
Spontaneous activity		
Genotype	$F(1,167) = 4.274$, $P = 0.04$	$F(1,333) = 0.933$, $P = 0.335$
Age	$F(2,167) = 2.565$, $P = 0.08$	$F(2,333) = 12.938$, $P < 0.0001$
Genotype-age interactions	$F(2,167) = 4.928$, $P = 0.008$	$F(2,333) = 0.052$, $P = 0.949$
Minimum threshold		
Genotype	$F(1,164) = 2.915$, $P = 0.09$	$F(1,331) = 6.436$, $P = 0.012$
Age	$F(2,164) = 13.385$, $P < 0.0001$	$F(2,331) = 12.583$, $P < 0.0001$
Genotype-age interactions	$F(2,164) = 1.274$, $P = 0.282$	$F(2,331) = 1.211$, $P = 0.299$
Response magnitude MT + 15 dB		
Genotype	$F(1,157) = 14.878$, $P = 0.00016$	$F(1,316) = 0.002$, $P = 0.968$
Age	$F(2,157) = 1.256$, $P = 0.288$	$F(2,316) = 6.132$, $P = 0.002$
Genotype-age interactions	$F(2,157) = 0.277$, $P = 0.759$	$F(2,316) = 1.534$, $P = 0.217$
Response magnitude MT + 30 dB		
Genotype	$F(1,155) = 18.529$, $P = 0.000030$	$F(1,314) = 0.041$, $P = 0.840$
Age	$F(2,155) = 1.625$, $P = 0.2$	$F(2,314) = 5.390$, $P = 0.005$
Genotype-age interactions	$F(2,155) = 2.117$, $P = 0.124$	$F(2,314) = 5.174$, $P = 0.006$

MT, minimum threshold; CF, characteristic frequency. Underscoring indicates significant values.

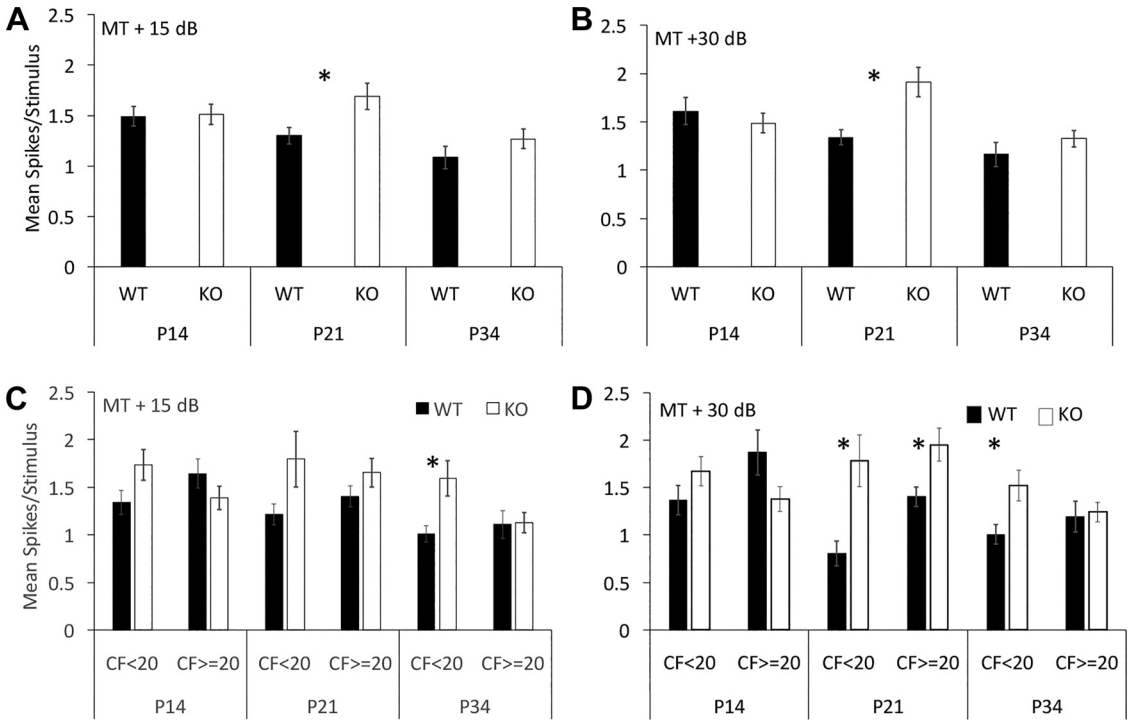

Fig. 5. *Fmr1* knockout (KO) inferior colliculus (IC) neurons show increased response magnitude to characteristic frequency (CF) tones than wild-type (WT) neurons. *A*: average response magnitude when tested with CF tones at 15 dB above minimum threshold (MT + 15 dB). There was a significant main effect of genotype and age ($P = 0.022$, $P = 0.002$, respectively) but no significant interaction between genotype × age ($P = 0.225$). *B*: average response magnitude when tested with CF tones at 30 dB above minimum threshold (MT + 30 dB). There was a significant interaction between genotype × age ($P = 0.014$), main effect of genotype ($P = 0.029$), and main effect of age ($P = 0.002$). *C*: response magnitude at MT + 15 dB for neurons separated by CF (CF <20 kHz vs. CF ≥20 kHz). For neurons with CF <20 kHz, there was no significant genotype × age interaction ($P = 0.759$) or main effect of age ($P = 0.288$). A significant main effect of genotype ($P = 0.00016$) was present. For neurons with CF ≥20 kHz, there was a significant main effect of age ($P = 0.002$) but no significant genotype × age interaction ($P = 0.217$) or main effect of genotype ($P = 0.968$). *D*: response magnitude at MT + 30 dB for neurons separated by CF. For neurons with CF <20 kHz, there was no significant interaction between genotype × age ($P = 0.124$) or main effect of age ($P = 0.2$). There was a significant main effect of genotype ($P = 0.000030$). For neurons with CF ≥20 kHz, there was a significant interaction between genotype × age ($P = 0.006$) and main effect of age ($P = 0.005$), but there was no significant main effect of genotype ($P = 0.840$). Error bars show SE. *$P < 0.05$.

MT + 30 dB (Fig. 5*D*), there was a significant main effect of genotype (Fig. 5*D*) but no main effect of age or genotype × age interactions.

For neurons with CF ≥20 kHz, response magnitude for tones presented at MT + 15 dB, (Fig. 5*C*) showed a main effect of age. There were no significant differences in Bonferroni post hoc comparison of P14 versus P21 ($P = 1.00$), but a significant difference was present for the P14 versus P34 ($P = 0.022$) and P21 versus P34 ($P = 0.003$) comparisons. There was no main effect of genotype or genotype × age interactions. At MT + 30 dB (Fig. 5*D*), there was no main effect of genotype. There was a main effect of age with no significant difference using Bonferroni post hoc comparisons in P14 versus P21 ($P = 1.000$) and P14 versus P34 ($P = 0.092$) but a significant difference in P21 versus P34 comparisons ($P = 0.003$). A significant genotype × age interaction was also present.

Overall, the number of action potentials elicited by the CF tone was higher in IC of *Fmr1* KO mice for neurons with CF <20 kHz. IC neurons with CF ≥20 kHz showed a reduction in response magnitude with age but no genotype differences. These results were similar to those seen with spontaneous activity.

Rate-level functions of IC neurons are not different between genotypes. Higher response magnitude at lower sound levels may predispose the *Fmr1* KO mice to AGS at high sound levels (Faingold et al. 1991). To quantify the relationship between increasing sound levels and response magnitude, rate-level functions were plotted for CF tone responses measured with sound levels between 10- and 90-dB SPL (e.g., Fig. 6*A*). Percent turnover (%TO) is a measure of the non-monotonicity of rate-level functions and indicates the extent to which responses are reduced after reaching a peak with increasing sound levels. We hypothesized that %TO is lower in *Fmr1* KO mice compared with WT mice. The dynamic range (DR) is the range of sound levels over which the response increases from 10% to 90% of maximum. We tested the hypothesis that DR was narrower in the *Fmr1* KO mouse IC than in WT mice. This would cause the *Fmr1* KO mouse IC to be activated to near maximal levels even with small increases in sound level.

When all neurons were combined across CF (Fig. 6*B*), there was no main effect of genotype in the %TO [$F(1,482) = 0.559$, $P = 0.455$] or genotype × age interactions ($F(2,482) = 0.716$, $P = 0.489$). There was a significant effect of age ($F(2,482) = 6.422$, $P = 0.002$) with Bonferroni post hoc significant differences at P14 versus P21 ($P = 0.011$) and P14 versus P34 ($P = 0.004$) but not at P21 versus P34 ($P = 1.00$). Percent TO decreased with age, indicating that neurons become more monotonic with age. For DR as well (Fig. 6*C*), there was no main effect of genotype [$F(1,356) = 0.601$, $P = 0.439$] or genotype × age interactions [$F(2,356) = 1.935$, $P = 0.146$].

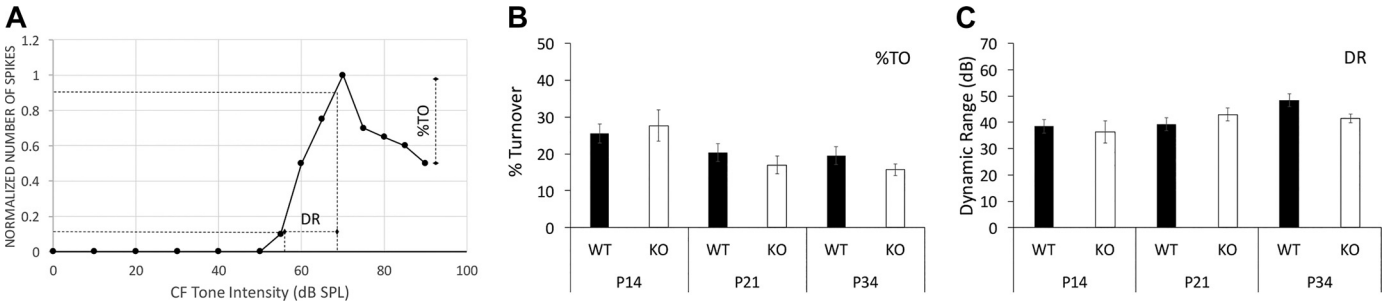

Fig. 6. Rate-level responses of inferior colliculus (IC) neurons were mostly unaffected by genotype at all ages tested. *A*: an example rate-level response function in a wild-type (WT) IC neuron [postnatal day (P)21]. Vertical dashed lines from left to right indicate sound level for 10% of maximum response and 90% of maximum response. Dynamic range (DR) was the range of sound levels over which responses increased from 10% to 90% of the maximum response. Percent turnover (%TO) is the degree of nonmonotonicity of the rate-level function and measures the extent to which response at the highest sound level tested is reduced compared with the maximum response. In this example, the %TO was ~50%. *B*: for %TO, there was no significant genotype × age interaction ($P = 0.489$) or main effect of genotype ($P = 0.455$). There was a main effect of age ($P = 0.002$), with neurons showing reduced %TO (less nonmonotonic) with age. *C*: dynamic range of neurons showed a main effect of age ($P = 0.031$) but no significant genotype × age interaction ($P = 0.146$) or main effect of genotype ($P = 0.439$). Error bars show SE.

There was a main effect of age [$F(2,356) = 3.522$, $P = 0.031$]. Bonferroni post hoc comparisons did not show any specific pairwise differences [P14 vs. P21, $P = 0.189$; P14 vs. P34, $P = 0.129$; and P21 vs. P34, $P = 1.00$].

When the data were split by CF (Table 3), the statistical trends were similar to those observed for the full data set. For %TO, neurons with CF <20 kHz showed no main effects of genotype or genotype × age interaction. There was a main effect of age with Bonferroni post hoc comparisons showing no significant pairwise differences (P14 vs. P21, $P = 0.061$; P14 vs. P34, $P = 0.138$; and P21 vs. P34, $P = 1.00$). For neurons with CF≥20 kHz, there was a decrease in %TO in *Fmr1* KO mice compared with WT mice. This indicates neurons were more monotonic in WT mice, in a disagreement with our original hypothesis. There was no significant genotype × age interaction or main effect of age. For the dynamic range measurement, neurons with CF <20 kHz showed no main effect of genotype or genotype × age interaction. There was a significant main effect of age with Bonferroni post hoc comparisons showing differences between P14 and P21 ($P = 0.004$) and P14 and P34 ($P = 0.013$) but not between P21 and P34 ($P = 1.00$). For neurons with CF ≥20 kHz, there were no main effects or interactions. Taken together, these data suggest that rate-level relationships in IC neurons were relatively normal in the *Fmr1* KO mice and may not contribute to auditory hypersensitivity in FXS.

Low-frequency IC neurons show longer response latency in Fmr1 KO mice. The median first spike latency of IC neuron responses to CF tone was measured at MT + 15 dB and MT + 30 dB (Fig. 7). For MT + 15 dB data, a two-way ANOVA showed a significant main effect of age for latency [$F(2, 477) = 35.43$, $P < 0.0001$, Fig. 7*A*]. There was no significant main effect of genotype [$F(1,477) = 0.613$, $P = 0.434$] or genotype × age interactions [$F(2,477) = 1.262$, $P = 0.284$]. Bonferroni post hoc analysis revealed a significant difference in the P14 versus P21 ($P < 0.0001$), P14 versus P34 ($P < 0.0001$), and P21 versus P34 ($P = 0.00082$) comparisons, with latencies decreasing with age. Likewise, for CF tones presented at MT + 30 dB (Fig. 7*B*), there was a significant main effect of age [$F(2,475) = 114.773$, $P < 0.0001$] with Bonferroni post hoc comparison at P14 versus P21 ($P < 0.0001$), P14 versus P34 ($P < 0.0001$), and P21 versus P34 ($P < 0.0001$) pairs, showing decreasing latency with age. There was no main effect of genotype [$F(1,475) = 0.904$, $P = 0.342$] or genotype × age interactions [$F(2, 475) = 0.087$, $P = 0.917$].

Table 3. *Statistical analysis of data classified according to CF (<20 kHz vs. ≥20 kHz) for percent turnover, dynamic range, and response latency to CF tones presented at MT + 15 dB and MT + 30 dB*

	CF <20 kHz	CF> = 20 kHz
Percent Turnover		
Genotype	$F(1,161) = 0.516$, $P = 0.473$	$F(1,330) = 4.368$, $P = 0.037$
Age	$F(2,161) = 3.624$, $P = 0.029$	$F(2,330) = 0.729$, $P = 0.483$
Genotype-age interactions	$F(2,161) = 0.405$, $P = 0.668$	$F(2,330) = 2.704$, $P = 0.068$
Dynamic range		
Genotype	$F(1,127) = 0.003$, $P = 0.959$	$F(1,223) = 0.011$, $P = 0.915$
Age	$F(2,127) = 8.188$, $P = 0.0004$	$F(2,223) = 0.053$, $P = 0.948$
Genotype-age interactions	$F(2,127) = 2.614$, $P = 0.077$	$F(2,223) = 1.719$, $P = 0.182$
Response latency at MT + 15 dB		
Genotype	$F(1,163) = 4.878$, $P = 0.029$	$F(1,315) = 3.430$, $P = 0.065$
Age	$F(2,163) = 10.682$, $P = 0.000044$	$F(2,315) = 34.024$, $P < 0.0001$
Genotype-age interactions	$F(2,163) = 0.297$, $P = 0.743$	$F(2,315) = 0.130$, $P = 0.878$
Response latency at MT + 30 dB		
Genotype	$F(1,143) = 4.128$, $P = 0.044$	$F(1,312) = 0.253$, $P = 0.615$
Age	$F(2,143) = 44.573$, $P < 0.0001$	$F(2,312) = 65.186$, $P < 0.0001$
Genotype-age interactions	$F(2,143) = 1.405$, $P = 0.249$	$F(2,312) = 0.045$, $P = 0.956$

MT, minimum threshold; CF, characteristic frequency.

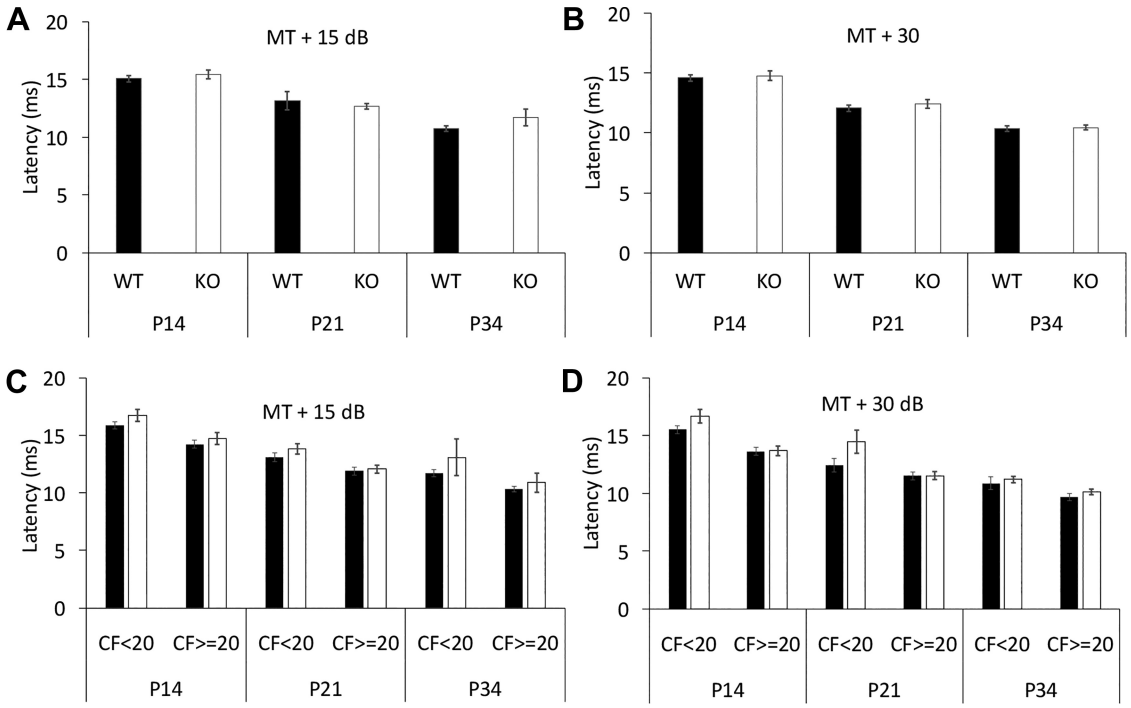

Fig. 7. No genotype differences were observed in median first spike latencies of neuronal response to characteristic frequency (CF) tones. *A*: the median first spike latency of responses to CF tone presented at minimum threshold (MT) + 15 dB showed no significant interaction between genotype × age ($P = 0.284$) or main effect of genotype ($P = 0.434$). There was a significant main effect of age ($P < 0.0001$), with latency decreasing with age. *B*: for latencies in response to CF tones at MT + 30 dB, there was no significant genotype × age interaction ($P = 0.917$) or main effect of genotype ($P = 0.342$). There was a significant main effect of age ($P < 0.0001$), with latencies decreasing with age. *C*: for neurons with CF <20 kHz, there was no significant interaction between genotype × age ($P = 0.743$) for latencies measured with tones presented at MT + 15 dB. However, there was a significant main effect of genotype ($P = 0.029$) and main effect of age ($P < 0.0001$). For neurons with CF ≥20 kHz, there was a significant main effect of age ($P < 0.001$) but no significance in genotype × age interaction or main effect of genotype ($P = 0.878$, $P = 0.065$, respectively). *D*: when tested with tones presented at MT+ 30 dB, the median first spike latency for neurons with CF <20 kHz showed significant main effect of genotype and age ($P = 0.044$, $P < 0.0001$, respectively) but no significant genotype × age interactions ($P = 0.249$). For neurons with CF ≥20 kHz, there was a significant main effect of age ($P < 0.0001$) but no significant main effect of genotype ($P = 0.615$) or genotype × age interaction ($P = 0.956$). Error bars show SE.

When neurons were classified by CF (Table 3), neurons with CF <20 kHz showed a significant main effect of genotype with longer latency in the KO compared with WT for tones with sound level of MT + 15 dB (Fig. 7*C*). There was also a main effect of age with Bonferroni post hoc comparison of P14 versus P21 ($P = 0.0042$), P14 versus P34 ($P = 0.00018$), and P21 versus P34 ($P = 1.00$) pairs, showing decreasing latency with age. There was no significant difference in genotype × age interaction. For neurons with CF ≥20 kHz, there was no significant main effect of genotype or genotype × age interactions. There was a significant main effect of age with Bonferroni post hoc analysis showing differences for P14 versus P21 ($P < 0.0001$), P14 versus P34 ($P < 0.0001$), and P21 versus P34 ($P = 0.0053$) pairs, with latency decreasing with age.

Similarly, at MT + 30 dB (Fig. 7*D*), neurons with CF <20 kHz showed a main effect of genotype and a main effect of age ($P < 0.0001$) with Bonferroni post hoc comparisons showing differences for the P14 versus P21 ($P = 0.0023$), P14 versus P34 ($P < 0.0001$), and P21 versus P34 ($P = 0.000055$) pairs, with latency decreasing with age. There was no significant genotype × age interaction. For neurons with CF ≥20 kHz, there was a significant main effect of age with Bonferroni post hoc comparisons showing differences for the P14 versus P21 ($P < 0.0001$), P14 versus P34 ($P < 0.0001$), and P21 versus P34 ($P < 0.0001$) pairs, with latencies decreasing with age. There was no significant main effect of genotype or genotype × age interactions. Thus the median first spike latency in response to CF tones decreased during development across all CFs, with genotype differences (slower latency in *Fmr1* KO neurons) seen for neurons with CF <20 kHz.

Low-frequency IC neurons in the Fmr1 KO mice show broader frequency tuning. To determine if frequency selectivity is affected in the IC of *Fmr1* KO mice, we performed a genotype and age comparison of frequency response area bandwidths (BW) at three different sound levels: 10, 20, and 30 dB above MT (BW10, BW20, and BW30, respectively). Frequency response areas (e.g., Fig. 8*A*) were plotted by measuring the number of action potentials to 20 repetitions of each frequency/sound level combination ranging from 4 to 48 kHz (4-Hz steps) and 10–90 dB SPL (10-dB steps). The bandwidth of the frequency response area at 10 (BW10), 20 (BW20), and 30 (BW30) dB above the neuron's MT was measured to quantify frequency selectivity.

For BW10, there was a significant genotype × age interaction [$F(2,307) = 4.971$, $P = 0.008$; Fig. 8*B*] but no main effect of genotype [$F(1,307) = 0.679$, $P = 0.410$] or age [$F(2,307) = 2.556$, $P = 0.079$]. A main effect of genotype was seen for BW20 (Fig. 8*B*), with broader tuning curves in *Fmr1* KO mice compared with WT mice [$F(1,307) = 3.927$, $P = 0.048$]. There was also a significant main effect of age [$F(2,307) = 6.096$, $P = 0.003$] with Bonferroni post hoc test showing a significant difference in P14 versus P21 ($P =$

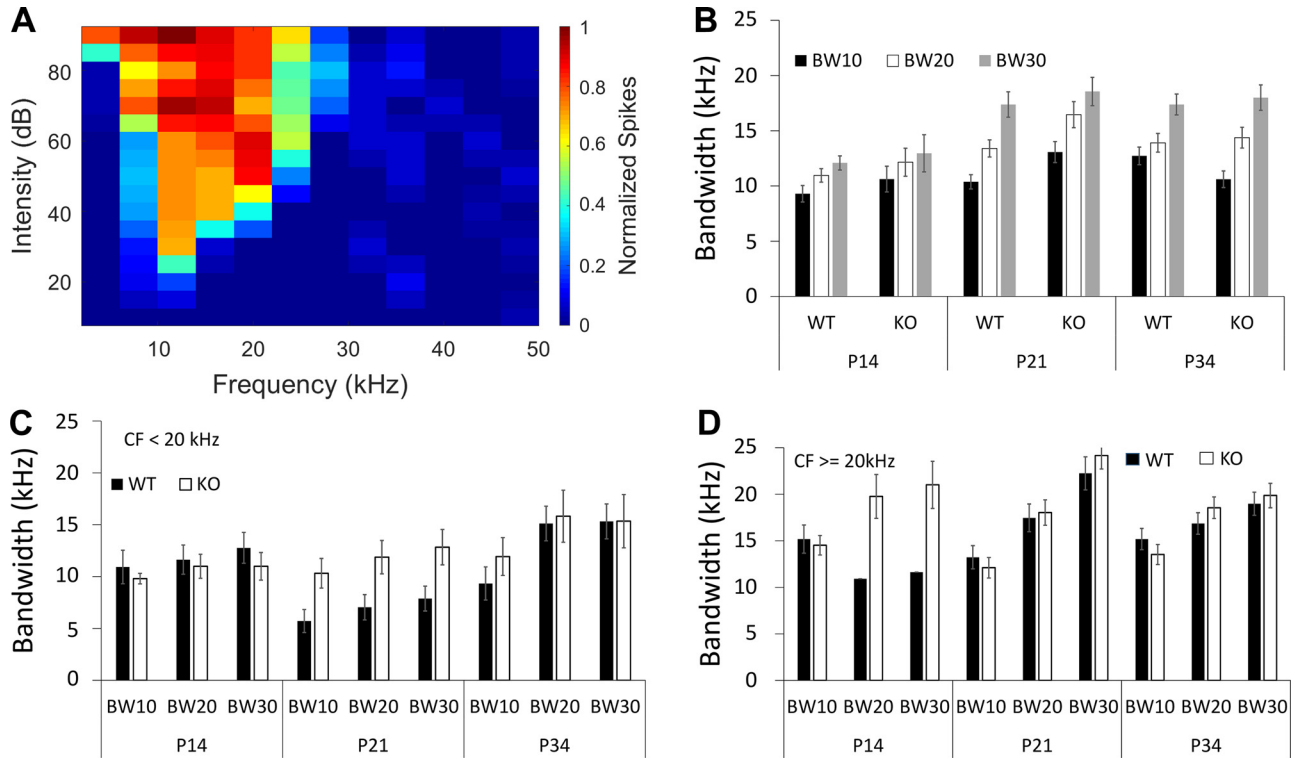

Fig. 8. Frequency tuning was broader in the inferior colliculus (IC) of *Fmr1* knockout (KO) mice compared with wild-type (WT) mice, mainly for neurons with CF <20 kHz. *A*: an example frequency response area with tone frequency on the abscissa and sound intensity on the ordinate. The color scale indicates normalized response magnitude for specific frequency-intensity combinations. The bandwidth of frequency selectivity was quantified at 10 (BW10), 20 (BW20), and 30 (BW30) dB above the minimum threshold of neurons. *B*: when all neurons within each genotype were pooled together, there was no significant main effect of genotype for BW10 ($P = 0.410$) or BW20 ($P = 0.354$). A significant main effect of genotype was present only for BW20 ($P = 0.048$). A significant main effect of age was seen for BW20 ($P = 0.003$) and BW30 ($P < 0.0001$) but not for BW10 (0.079). *C*: For neurons with CF <20 kHz, there was a significant main effect of genotype [BW10 ($P = 0.039$), BW20 ($P = 0.017$), and BW30 ($P = 0.018$)]. There was no genotype × age interaction [BW10 ($P = 0.175$), BW20 ($P = 0.616$), and BW30 ($P = 0.68$)] or main effect of age [BW10 ($P = 0.944$), BW20 ($P = 0.515$), and BW30 ($P = 0.288$)]. *D*: for neurons with CF ≥20 kHz, there was no significant main effect of genotype ($P = 0.726$) or age ($P = 0.499$). There was a significant genotype × age interaction only for BW10 ($P = 0.04$). Error bars show SE.

0.002) and P14 versus P34 ($P = 0.024$) but not P21 versus P34 ($P = 1.00$). There was no significant genotype × age interaction [$F(2,307) = 1.095$, $P = 0.336$]. For BW30 (Fig. 8*B*), there was a significant effect of age [$F(2,307) = 12.276$, $P = 0.000007$] with Bonferroni post hoc showing a difference in P14 versus P21 ($P = 0.000018$) and P14 versus P34 ($P = 0.000066$) but not in the P21 versus P34 ($P = 1.00$) groups. There was no main effect of genotype [$F(1,307) = 0.860$, $P = 0.354$] or genotype × age interaction [$F(2,307) = 0.032$, $P = 0.968$]. Thus, when all neurons were considered together, genotype difference was seen only for BW20 with *Fmr1* KO neurons showing broader tuning. For BW20 and BW30, we observed a narrowing of tuning curves with developmental age.

When separated by CF, neurons with CF <20 kHz (Fig. 8*C* and Table 4) were more broadly tuned in the *Fmr1* KO IC compared with WT IC at BW10, BW20, and BW30. For BW10, BW20, and BW30, there was no significant genotype × age interaction or

Table 4. *Statistical analysis of data classified according to CF (<20 kHz vs. ≥20 kHz)*

	CF <20 kHz	CF ≥20 kHz
BW10		
Genotype	$F(1,118) = 4.346$, $P = 0.039$	$F(1,181) = 0.123$, $P = 0.726$
Age	$F(2,118) = 0.058$, $P = 0.944$	$F(2,181) = 0.699$, $P = 0.499$
Genotype-age interactions	$F(2,118) = 1.771$, $P = 0.175$	$F(2,181) = 3.272$, $P = 0.04$
BW20		
Genotype	$F(1,118) = 5.9$, $P = 0.017$	$F(1,182) = 1.221$, $P = 0.271$
Age	$F(2,118) = 0.487$, $P = 0.515$	$F(2,182) = 2.606$, $P = 0.077$
Genotype-age interactions	$F(2,118) = 0.487$, $P = 0.616$	$F(2,182) = 0.497$, $P = 0.609$
BW30		
Genotype	$F(1,116) = 5.806$, $P = 0.018$	$F(1,180) = 0.225$, $P = 0.636$
Age	$F(2,116) = 1.259$, $P = 0.288$	$F(2,180) = 4.013$, $P = 0.20$
Genotype-age interactions	$F(2,116) = 0.387$, $P = 0.68$	$F(2,180) = 0.702$, $P = 0.497$

BW10, BW20, and BW30, bandwidth at MT + 15 dB, MT + 20 dB, and MT + 30 dB, respectively; MT, minimum threshold; CF, characteristic frequency; BW, bandwidth.

main effect of age. Neurons with CF ≥20 kHz (Fig. 8*D*) showed no main genotype or age effects for BW10, BW20, or BW30. A genotype × age interaction was only seen for BW10. Thus IC neurons with CF <20 kHz, but not higher CF neurons, showed a broader tuning in *Fmr1* KO compared with WT mice, which was more pronounced at P21. Yet again, these data indicate that IC neurons with CF <20 kHz show more genotype differences than neurons with CF ≥20 kHz.

IC neurons showed stronger responses to amplitude modulated tones in Fmr1 KO than WT mice. The rate modulation transfer function (rMTF) and temporal modulation transfer function (tMTF) for responses to sinusoidal amplitude modulated (SAM) tones were compared across age and genotype (Fig. 9). The rMTF was analyzed as the average number of spikes per stimulus presentation over the duration of the stimulus. The tMTF was quantified as the degree of synchronization to the modulations measured as vector strengths. Modulation rates of 5, 10, 20, 50, 100, and 200 Hz with carrier frequency centered at CF were used and the SAM tone was presented at MT + 15 dB.

For rMTF analysis, a two-way ANOVA (genotype and age as factors) was run for each modulation rate. The main statistics are summarized in Table 5, including analyses of all neurons pooled or separated by CF (20 kHz cut-off). In general, Table 5 and Figs. 9 and 10 show a number of significant genotype differences in rMTF driven mostly by increased responses to SAM in the *Fmr1* KO mice. Figure 9 also suggests that the increased responses are more prominent at faster modulation rates with *Fmr1* KO IC neurons showing a peak ~50-Hz modulation rates compared with WT neurons, on average. Neurons with CF <20 kHz also show more consistent genotype differences across modulation rates (Table 5 and Fig. 10). No consistent patterns were seen for main effects of age or age × genotype interactions. Together, we interpret these data to indicate that responses to modulated tones are increased in the *Fmr1* KO mice.

For tMTF (Table 6 and Figs. 9, 11), main effects of genotype were rare (seen only for 10 Hz modulation rate), and the other effects do not show a consistent pattern of specific developmental change or genotype × age interactions. This suggests that temporal response properties of IC neurons when tested with SAM tones are not different in *Fmr1* KO mice compared with WT and are unlikely to contribute to abnormal auditory sensitivity.

Tonotopy. We quantified the development and possible genotype differences in tonotopy in the IC and observed the expected dorsal to ventral increase in CF representation (Felix and Portfors 2007) at all three developmental ages (Fig. 12) and across genotypes. The CF representation was mostly <30 kHz at P14 and expanded to include more neurons with CF >30 kHz at P21 and P34. There was no significant difference in the distribution of CFs across genotypes at any age [P14: $t(159) = 0.831$, $P = 0.406$; P21: $t(164) = 0.788$, $P = 0.431$; and P34: $t(188) = 0.589$, $P = 0.555$]. Together, these data suggest that CF-specific susceptibilities in *Fmr1* KO mice are not due to abnormal development of tonotopy.

DISCUSSION

Based on c-Fos+ cell density analysis, our results indicate that more IC neurons were activated in the *Fmr1* KO mice compared with WT following sound exposure at both P21 and P34. Genotype differences in the density of c-Fos+ cells are also observed in the PP and SGN divisions of the MGB. In vivo single unit recordings show that IC neurons of *Fmr1* KO mice are more responsive to both tone bursts and amplitude-

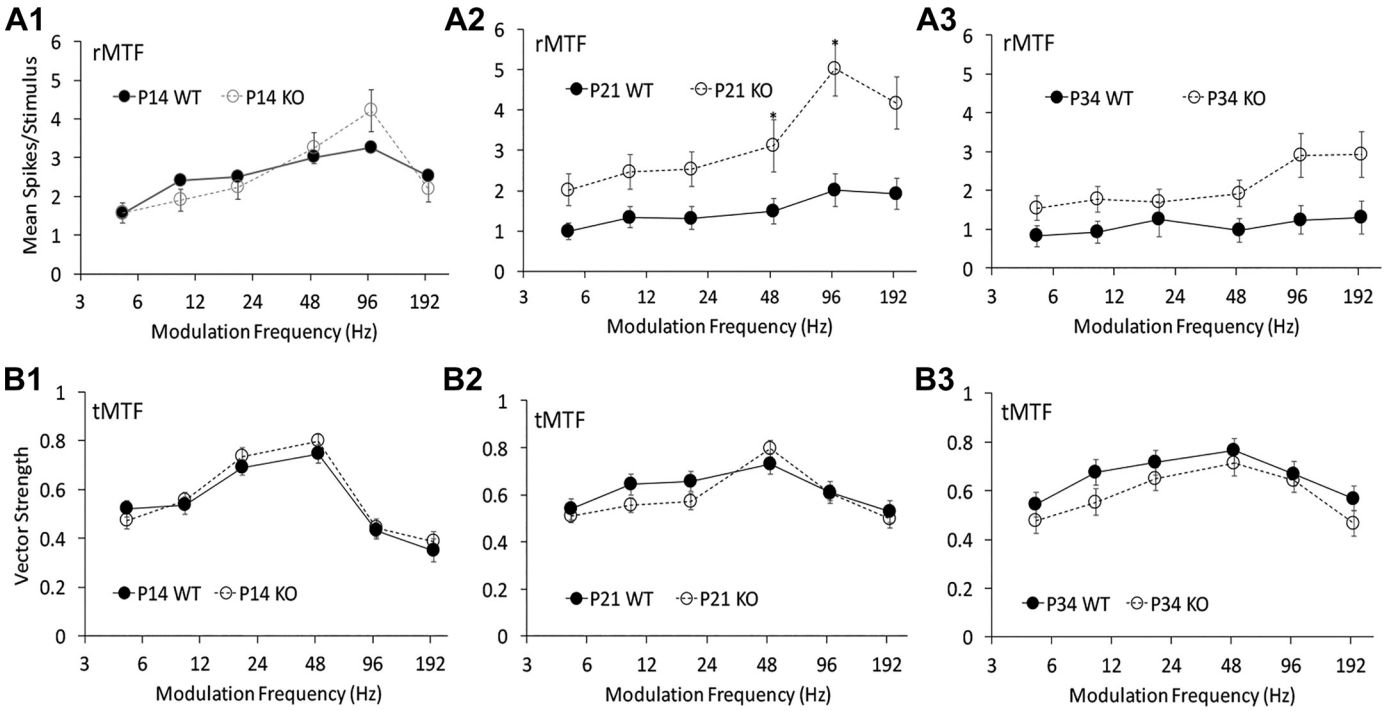

Fig. 9. Inferior colliculus (IC) neurons show hyperresponsiveness to amplitude modulated tones in *Fmr1* knockout (KO) mice, but phase-locking is normal. *A1–A3*: rate modulation transfer function (rMTF) in the P14, P21, and P34 groups, respectively. *B1–B3*: temporal modulation transfer function (tMTF) in the P14, P21, and P34 groups, respectively. Dashed lines indicate *Fmr1* KO mice and solid lines indicate WT mice. Error bars show SE. *$P < 0.05$.

Table 5. *Statistical analysis of rate modulation transfer functions obtained from WT and Fmr1 KO mice at the three developmental time points*

Modulation Frequency/CF Frequency	Genotype × Age Interaction	Main Effect of Genotype	Main Effect of Age
5 Hz			
All	$F(2,412) = 1.973$, $P = 0.140$	$F(1,412) = 2.011$, $P = 0.157$	$F(2,412) = 0.688$, $P = 0.503$
CF <20 kHz	$F(2,159) = 1.697$, $P = 0.187$	$F(1,159) = 7.366$, $P = 0.007$*	$F(2,159) = 0.832$, $P = 0.437$
CF ≥20 kHz	$F(2,315) = 3.264$, $P = 0.040$*	$F(2,315) = 0.001$, $P = 0.972$	$F(2,315) = 4.279$, $P = 0.015$*
10 Hz			
All	$F(2,406) = 1.028$, $P = 0.359$	$F(1,406) = 0.573$, $P = 0.450$	$F(2,406) = 1.119$, $P = 0.328$
CF <20 kHz	$F(2,159) = 1.952$, $P = 0.145$	$F(2,159) = 2.046$, $P = 0.155$	$F(2,159) = 0.337$, $P = 0.715$
CF ≥20 kHz	$F(2,314) = 1.224$, $P = 0.296$	$F(2,314) = 0.641$, $P = 0.424$	$F(2,314) = 2.351$, $P = 0.097$
20 Hz			
All	$F(2,415) = 0.733$, $P = 0.481$	$F(1,415) = 5.389$, $P = 0.021$*	$F(2,415) = 4.455$, $P = 0.012$*
CF <20 kHz	$F(2,159) = 2.732$, $P = 0.068$	$F(1,159) = 5.786$, $P = 0.017$*	$F(2,159) = 1.389$, $P = 0.252$
CF ≥20 kHz	$F(2,314) = 0.334$, $P = 0.717$	$F(1,314) = 2.600$, $P = 0.108$	$F(2,314) = 11.143$, $P < 0.0001$*
50 Hz			
All	$F(2,414) = 1.538$, $P = 0.216$	$F(1,414) = 16.72$, $P < 0.0001$*	$F(2,414) = 3.378$, $P = 0.035$*
CF <20 kHz	$F(2,159) = 1.778$, $P = 0.172$	$F(2,159) = 5.013$, $P = 0.027$*	$F(2,159) = 1.008$, $P = 0.367$
CF ≥20 kHz	$F(2,315) = 1.387$, $P = 0.251$	$F(2,315) = 11.473$, $P = 0.001$*	$F(2,315) = 6.064$, $P = 0.003$*
100 Hz			
All	$F(2,410) = 2.704$,$P = 0.068$	$F(1,410) = 6.729$, $P = 0.010$*	$F(2,410) = 1.292$, $P = 0.276$
CF <20 kHz	$F(2,159) = 3.724$, $P = 0.026$*	$F(2,159) = 6.828$, $P = 0.010$*	$F(2,159) = 0.367$, $P = 0.693$
CF ≥20 kHz	$F(2,293) = 2.813$, $P = 0.062$	$F(1,293) = 1.760$, $P = 0.186$	$F(2,293) = 1.599$, $P = 0.204$
200 ;Hz			
All	$F(2,401) = 2.282$, $P = 0.103$	$F(2,401) = 1.845$, $P = 0.175$	$F(2,401) = 0.262$, $P = 0.770$
CF <20 kHz	$F(2,159) = 5.217$, $P = 0.023$*	$F(2,159) = 5.217$, $P = 0.024$*	$F(2,159) = 0.413$, $P = 0.663$
CF ≥20 kHz	$F(2,314) = 1.709$, $P = 0.183$	$F(1,314) = 0.348$, $P = 0.556$	$F(2,314) = 1.52$, $P = 0.220$

Data are organized according to the modulation frequency. "All" indicates all the neurons combined. Characteristic frequencies (CF) <20 kHz and CF ≥20 kHz indicate when data were split according to CF. MT, minimum threshold; WT, wild type; KO, knockout. *$P < 0.05$.

modulated tones and show broader frequency tuning curves than their WT counterparts. In general, genotype differences emerge between P14 and P21, with a stronger effect on neurons with CF<20 kHz, compared with neurons with higher CF. Together, these data suggest that the IC is a major contributor to early developmental auditory hyperresponsiveness in FXS.

Increased density of c-Fos+ cells in the IC of Fmr1 KO mice at both P21 and P34. The genotype difference in c-Fos+ cell density was apparent in the dorsolateral half of the IC at P21 and shifted to the ventromedial half of the IC (adjacent to the periaqueductal gray) at P34. Chen and Toth (2001) previously examined c-Fos expression in response to sounds in *Fmr1* KO mice using sound levels that caused AGS in some of the mice. When AGS was induced in *Fmr1* KO mice, there was an increase in c-Fos expression in KO compared with WT mice in the dorsal nucleus of the lateral lemniscus, posterior intralaminar nucleus, periaqueductal gray, and MGm. However, because the *Fmr1* KO mice showed seizures and the WT mice did not, motor responses associated with increased AGS-related movement likely contributed to the genotype differences in c-Fos+ cell density (Yang et al. 2020). To overcome this confound, the sound stimulus in our study was in the 80- to 90-dB range, which did not induce AGS in any of the mice used for c-Fos analysis. Under these conditions, we found a genotype difference in the density of c-Fos+ cells in the IC suggesting that the extent of activity in the IC may be a correlate of sensory hypersensitivity in early development.

Dorsomedial IC represents low CFs while ventromedial IC represents higher CFs. Hyperresponsiveness is seen in *Fmr1* KO IC in response to both tone bursts and AM tones for neurons with CF <20 kHz at both P21 and P34. Neurons with CF ≥20 kHz do not show considerable differences in response magnitude at either P21or P34. This lack of spatiotemporal correlation between the c-Fos data and single unit data suggests that the increased density of c-Fos+ cells and increased response magnitudes may contribute independently to hypersensitivity.

Analysis of the density of c-Fos+ cells in the MGB suggests a point of interaction between abnormal sensory processing and anxiety in FXS during early development (Cho et al. 2011). The MGm is a region projecting to all cortical layers and to the amygdala. The SGN is a region that receives multisensory inputs and also projects to the amygdala (LeDoux et al. 1991). The peripeduncular (PP) nucleus integrates auditory, motor, and hypothalamic signals (Arnault and Roger 1987). The recruitment of more cells may underlie a stronger activation of auditory-limbic-motor pathways that may lead to behavioral anxiety phenotypes in response to daily environmental sounds in FXS (Miller et al. 1999; Reinhard et al. 2019).

We did not observe an increase in sound-evoked c-Fos+ cell density in the auditory cortex at P21 or P34. While the IC showed both higher density of activated c-Fos+ cells and increased response magnitude in the *Fmr1* KO mice at this age, the auditory cortex only shows the increased response magnitude (Wen et al. 2018). When *Fmr1* KO mice are most sensitive to AGS (~P21), our data suggest that the IC plays a stronger role than the cortex. This is consistent with the role of IC in AGS generation in rats genetically prone to epilepsy (Faingold 2002) and in the *Fmr1* KO mice (Gonzalez et al. 2019).

Single unit recordings reveal hypersensitivity to sounds in the IC of Fmr1 KO mice. In vivo electrophysiological recordings in the IC at P14, P21, and P34 showed that the *Fmr1* KO

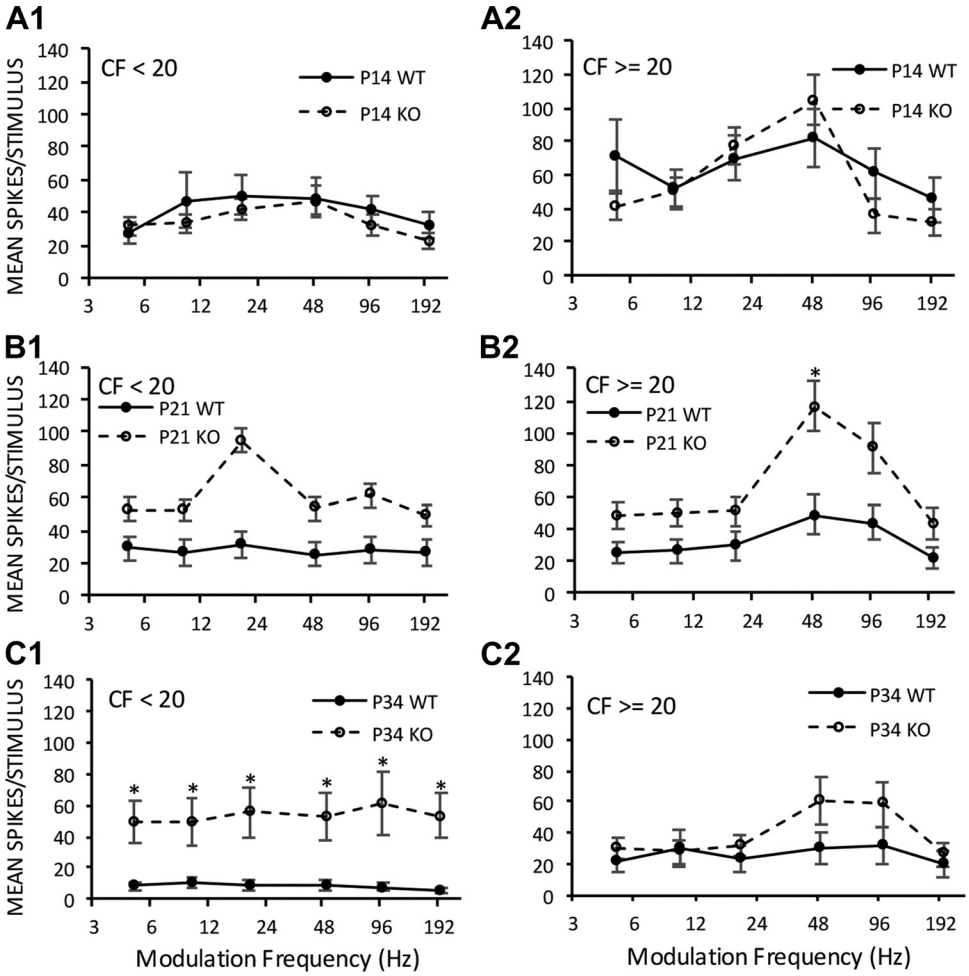

Fig. 10. Rate modulation transfer function (rMTF) subdivided into neurons with characteristic frequency (CF) <20 kHz (*A1*, *B1*, and *C1*) and CF ≥20 kHz (*A2*, *B2*, and *C2*). The rows are arranged by postnatal age (P14, P21, and P34). Error bars show SE. *$P < 0.05$).

neurons produce increased responses to tone bursts and amplitude-modulated tones and had broader frequency tuning curves compared with age-matched WT neurons. Low-frequency tuned neurons (CF <20 kHz) show greater genotype differences compared with neurons with CF ≥20 kHz. Rotschafer and Razak (2013) suggested that a possible mechanism of increased synchrony and hypersensitivity to sounds may be linked to broader frequency tuning curves of individual neurons in *Fmr1* KO mice. This is because more neurons would be activated in response to a single tone frequency if tuning curves were broader and overlapped more. IC neurons show broader tuning curves in *Fmr1* KO mice than in WT, suggesting that more IC neurons will respond synchronously to sounds. These data suggest that the IC is a major source of auditory hyperresponsiveness in FXS during development through increased response magnitudes and a greater number of synchronously activated neurons.

Faingold and Anderson (1991) suggested that abnormal inhibition with increasing sound level in IC neuronal response may lead to AGS in rats genetically susceptible to epilepsy. Therefore, we quantified rate-level responses across age and genotype. In the *Fmr1* KO mice, there were no genotype differences in either the nonmonotonicity of responses or the dynamic range. These data do not support the hypothesis that AGS susceptibility of *Fmr1* KO mice is due to abnormal rate-level relationships in the IC. Given the CF-specific genotype effects observed and because of a previous study that showed tonotopic gradients of ion channel expression may be affected in the lower auditory brainstem, we hypothesized that development of tonotopy may show genotype differences (Ruby et al. 2015; Strumbos et al. 2010). However, there were no genotype differences in tonotopy indicating that map formation and the underlying guidance cues (Cramer and Gabriele 2014) are relatively normal in the IC of *Fmr1* KO mice. Therefore, increased response to unmodulated and amplitude-modulated tones, broader frequency tuning curves, and increased recruitment of active cells seem to be the major IC phenotypes associated with auditory hyperresponsiveness at P21.

Development of IC responses in WT and Fmr1 KO mice. Although the major focus of our study was on the *Fmr1* KO mice, the WT data are useful to compare with previous studies of IC development. Our data are consistent with previous findings of shortening latencies, decreasing thresholds, sharpening frequency tuning, and increasing high-frequency representation in the developing IC (Aitkin and Moore 1975; Ehret and Romand 1992; Romand and Ehret 1990; Shnerson and Willott 1979). In addition, we show that both spontaneous and tone-driven response magnitudes of IC neurons decline with age. This was also true for responses to amplitude modulated tones. When IC neurons with CF <20 kHz are considered, there was no main effect of age on the rMTF to AM tones (Table 5). However, IC neurons with CF ≥20 kHz show reduced spike counts with age at multiple modulation rates.

Table 6. *Statistical analysis of the temporal modulation transfer functions obtained from WT and Fmr1 KO mice at the three developmental time points*

Modulation Frequency/CF Frequency	Genotype × Age Interaction	Main Effect of Genotype	Main Effect of Age
5 Hz			
All CF	$F(2,390) = 0.127$, $P = 0.881$	$F(2,390) = 2.872$, $P = 0.091$	$F(2,390) = 0.354$, $P = 0.702$
CF <20 kHz	$F(2,137) = 0.159$, $P = 0.853$	$F(1,137) = 0.472$, $P = 0.493$	$F(2,137) = 0.275$, $P = 0.760$
CF ≥20 kHz	$F(2,242) = 0.052$, $P = 0.949$	$F(1,242) = 2.777$, $P = 0.097$	$F(2,242) = 1.050$, $P = 0.351$
10 Hz			
All CF	$F(2,383) = 1.989$, $P = 0.138$	$F(1,383) = 4.912$, $P = 0.027$*	$F(2,383) = 2.001$, $P = 0.137$
CF <20 kHz	$F(2,136) = 0.905$, $P = 0.407$	$F(1,136) = 0.759$, $P = 0.385$	$F(2,136) = 3.110$, $P = 0.048$*
CF ≥20 kHz	$F(2,235) = 1.386$, $P = 0.252$	$F(1,235) = 4.241$, $P = 0.041$*	$F(2,235) = 0.695$, $P = 0.500$
20 Hz			
All CF	$F(2,387) = 2.353$, $P = 0.096$	$F(2,387) = 1.702$, $P = 0.193$	$F(2,387) = 4.997$, $P = 0.007$*
CF <20 kHz	$F(2,135) = 0.887$, $P = 0.414$	$F(1,135) = 1.069$, $P = 0.303$	$F(2,135) = 3.287$, $P = 0.040$*
CF ≥20 kHz	$F(2,240) = 2.087$, $P = 0.126$	$F(1,240) = 0.599$, $P = 0.440$	$F(2,240) = 1.734$, $P = 0.179$
50 Hz			
All CF	$F(2,382) = 2.058$, $P = 0.129$	$F(1,382) = 0.752$, $P = 0.386$	$F(2,382) = 0.609$, $P = 0.544$
CF <20 kHz	$F(2,129) = 0.918$, $P = 0.402$	$F(1,129) = 0.226$, $P = 0.636$	$F(2,129) = 0.836$, $P = 0.436$
CF ≥20 kHz	$F(2,241) = 0.819$, $P = 0.442$	$F(1,241) = 0.08$, $P = 0.778$	$F(2,241) = 1.173$, $P = 0.311$
100 Hz			
All CF	$F(2,388) = 0.153$, $P = 0.858$	$F(1,388) = 0.061$, $P = 0.804$	$F(2,388) = 22.195$, $P < 0.0001$*
CF <20 kHz	$F(2,130) = 0.502$, $P = 0.607$	$F(1,130) = 1.124$, $P = 0.291$	$F(2,130) = 8.009$, $P = 0.001$
CF ≥20 kHz	$F(2,248) = 0.356$, $P = 0.701$	$F(1,248) = 0.119$, $P = 0.731$	$F(2,248) = 12.587$, $P < 0.0001$*
200 Hz			
All CF	$F(2,352) = 1.356$, $P = 0.259$	$F(1,352) = 0.932$, $P = 0.335$	$F(2,352) = 9.349$, $P = 0.0001$*
CF <20 kHz	$F(2,120) = 0.433$, $P = 0.650$	$F(2,120) = 0.027$, $P = 0.870$	$F(2,120) = 4.008$, $P = 0.021$*
CF ≥20 kHz	$F(2,222) = 1.738$, $P = 0.178$	$F(1,222) = 1.245$, $P = 0.266$	$F(2,222) = 4.665$, $P = 0.010$*

Data are organized according to the modulation frequency. "All" indicates all the neurons combined. Characteristic frequencies (CF) <20 kHz and CF ≥20 kHz indicate when data were split according to CF. MT, minimum threshold; WT, wild type; KO, knockout. *$P < 0.05$.

This suggests that AM responses mature more slowly in the high-frequency IC neurons. Taken together, these data are in alignment with both the development of the cochlea and the maturation of inhibitory circuitry that shape frequency tuning and response magnitudes of IC neurons (Fuzessery and Hall 1996; Hurley et al. 2008; Le Beau et al. 1996; Zhang and Kelly 2003).

A number of age × genotype interactions were observed in this study suggesting that some of the differences may be present only at certain ages. A notably important pattern in the data was that the IC properties are comparable between *Fmr1* KO and WT mice at P14 but begin to diverge at P21. Sound-driven responses begin to occur ~P10–11 in the IC. In the first 2 wk of life, refinement of both extrinsic ascending and intrinsic local connectivity patterns depend mostly on spontaneous activity driven by the cochlea (Gabriele et al. 2000a). Patterns of extrinsic inputs to the IC appear mature at or before hearing onset (Fathke and Gabriele 2009; Gabriele et al. 2000b; Henkel et al. 2007). Our data suggest that this developmental process is relatively normal in *Fmr1* KO mice. Between P14 and P21, sound-driven refinements of excitatory local inputs dominate such that inhibition becomes relatively stronger (E:I ratio declines from P14–21 in WT mice, Sturm et al. 2014). This will sharpen frequency tuning and reduce response magnitudes during development. This process seems to be affected in *Fmr1* KO mice. Abnormal sound-driven refinement may result in elevated response magnitude, broader frequency tuning and consequently hypersensitivity. Grimsley et al. (2013) suggested that the local circuit connectivity may shape responses of IC neurons to increasing sound levels. Therefore, abnormal local IC circuit refinement may also be implicated in AGS. Whether this is due to abnormal refinement of excitatory connections and/or abnormal development of inhibition remains to be investigated.

Another main observation is that neurons with CF <20 kHz appear to be more hypersensitive than neurons with CF ≥20 kHz. The underlying mechanisms for this frequency dependence are unclear, but suggest abnormal GABA responses in the IC of *Fmr1* KO mice. Based on the IC tonotopic gradient, neurons with increasing CF are found more ventrally in the IC and most neurons with CF <20 kHz are likely to be within 1,000 μm from the dorsal surface (~50% of total dorso-ventral depth (Felix and Portfors 2007). IC neurons receive both GABA and glycine inhibitory inputs. Glycine may be more dominant in shaping inhibition in ventral, high-CF regions of the IC (Choy Buentello et al. 2015; Merchán et al. 2005; Sanes et al. 1987). GAD67-labeled inputs appear to dominate more in the dorso-medial regions of the IC (Choy Buentello et al. 2015), suggesting a more prominent role for GABA in the dorsal half of the IC. This may suggest a deficit in GABAergic inhibition, because most deficits were observed in low CF neurons in the dorsolateral region of the IC. GABAa receptor deficits in the IC are related to AGS in rats that are genetically susceptible to epilepsy (Faingold 2002). In addition, down-regulated tonic GABAa currents and a decrease in GABAa receptors were reported in *Fmr1* KO mice (Curia et al. 2009; D'Hulst et al. 2006), suggesting impaired GABA-mediated inhibition in FXS. GABAergic inputs shape firing rates of IC neurons (Palombi and Caspary, 1996). Whether glycinergic inhibition is affected in the IC is unclear, but Garcia-Pino et al. (2017) showed no impact on such inhibition in the lower brainstem of *Fmr1* KO mice. Together, these studies suggest the CF-dependent susceptibility of IC to hyperresponsiveness in early development may be related to GABA dysfunction in *Fmr1* KO mice.

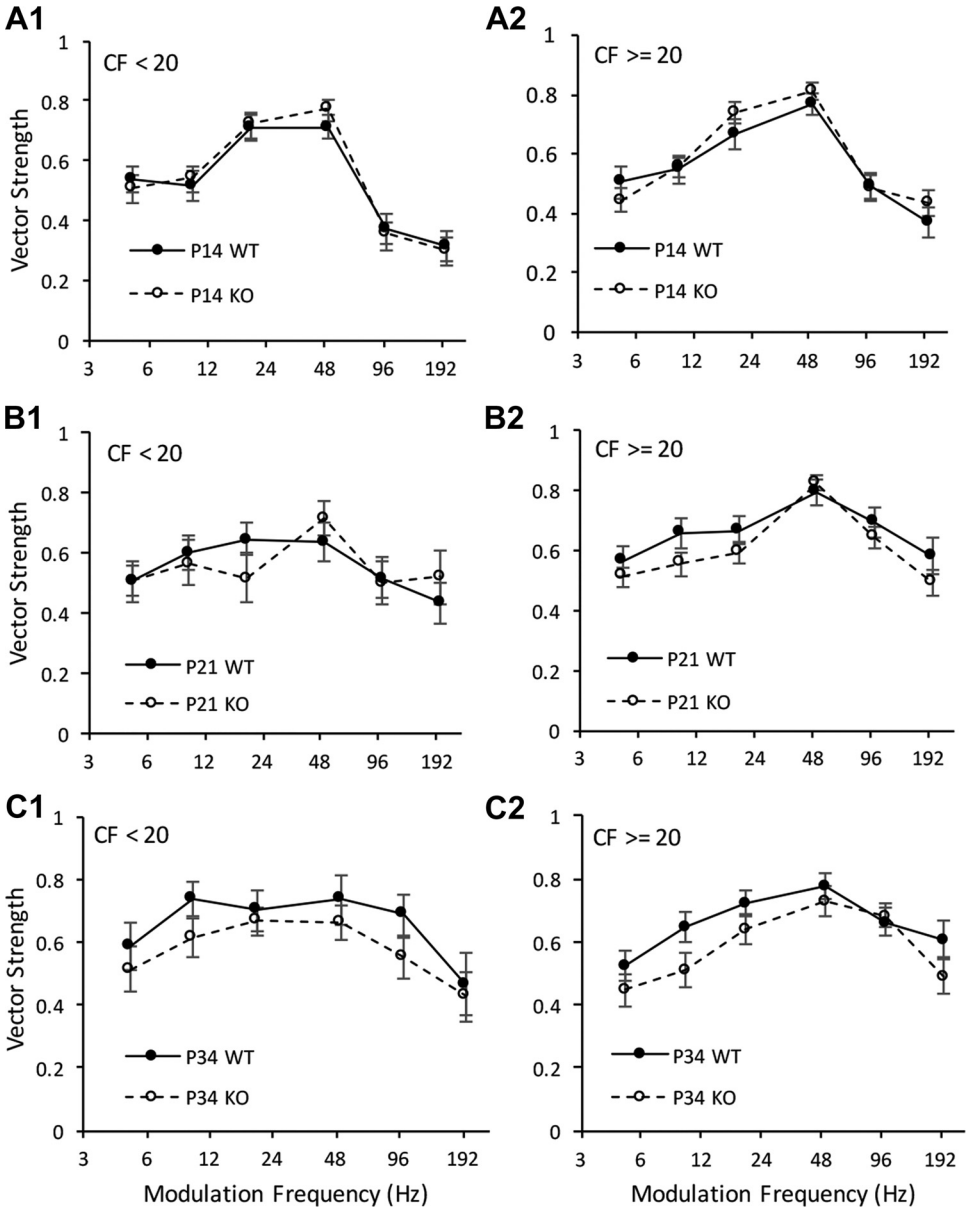

Fig. 11. Temporal modulation transfer function (tMTF) subdivided into neurons with characteristic frequency (CF) <20 kHz (*A1*, *B1*, and *C1*) and CF ≥20 kHz (*A2*, *B2*, and *C2*). The rows are arranged by postnatal age (P14, P21, and P34). Error bars show SE.

System-wide deficits in auditory processing in FXS. Given the consistent and debilitating auditory hypersensitivity in individuals with FXS, there is an increasing interest in understanding the underlying the circuit and cellular pathophysiology across the auditory system and across development (McCullagh et al. 2020). FMRP is expressed at multiple levels of the auditory system from the cochlear nucleus to the auditory cortex. Global deletion of *Fmr1* would affect the development and function of each of these auditory processing stages. Neurons in the lateral superior olive (LSO) of the brainstem show enhanced excitatory synaptic input strength through increased convergence of cochlear nucleus input early in development (Garcia-Pino et al. 2017). LSO neurons showed increased firing rates and broader frequency tuning curves. The abnormal IC responses may, therefore, originate in the lower brainstem. However, this needs to be verified by comparing lower brainstem and IC recordings conducted at similar ages. In the medial nucleus of the trapezoid body (MNTB), one of the major sources of inhibition to the LSO, the tonotopic gradient of Kv3.1b potassium ion channel is significantly flatter in *Fmr1* KO, compared with WT mice (Strumbos et al. 2010). Modeling (Strumbos et al. 2010) and electrophysiological (Brown et al. 2010) data suggest an impact on temporal precision in MNTB of *Fmr1* KO mice. This may be limited to the MNTB, as our IC data do not reveal any genotype differences in tMTF in response to amplitude modulated tones, suggesting that single neuron phase locking is not affected in the IC. Cell sizes were also reduced and VGAT expression is elevated in the MNTB of the *Fmr1* KO mice suggesting increased inhibitory input and disinhibition of the LSO (Rotschafer et al. 2015).

The auditory cortex has received considerable attention in FXS. Rotschafer and Razak (2013) showed increased response magnitude and broader frequency tuning in the auditory cortex of *Fmr1* KO mice. Wen et al. (2018) showed that such responses are seen at P21, but not at P14, suggesting the origin of hyperresponsivity in this developmental time frame when cortical properties mature (Oswald and Reyes 2008, 2011). The

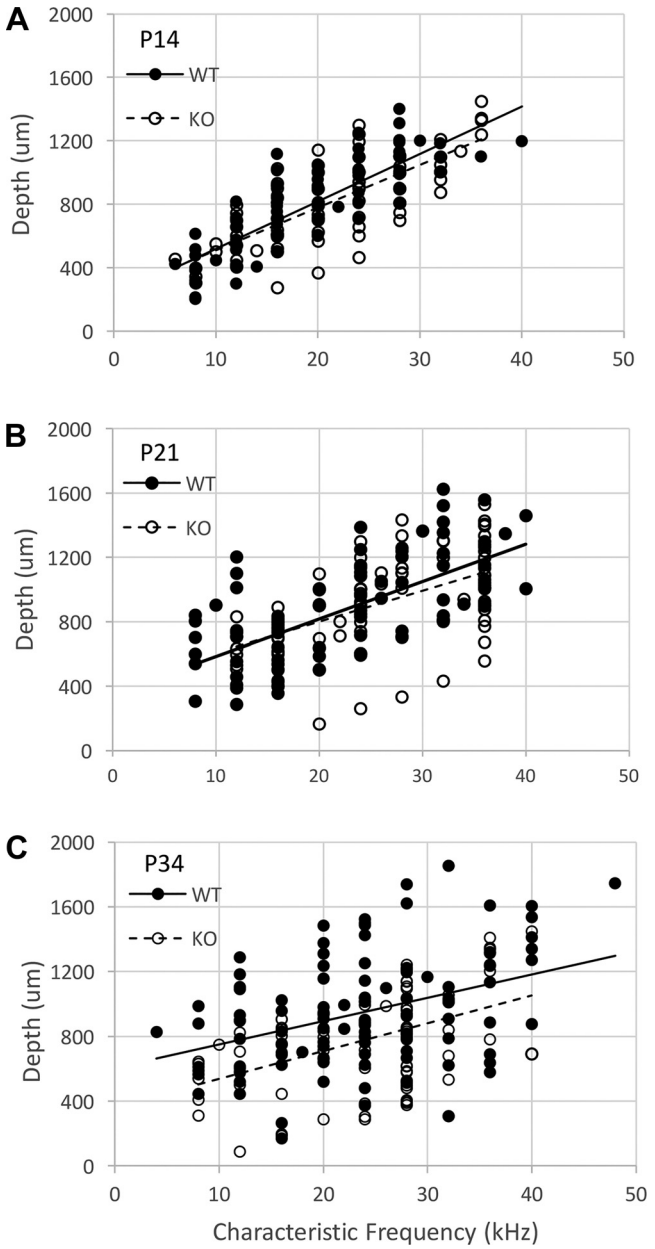

Fig. 12. No genotype differences were observed in inferior colliculus (IC) tonotopy at any age. Distribution of characteristic frequency (CF) along recording depth in the IC. There were no significant differences between wild-type (WT) and *Fmr1* knockout (KO) mice at each age group postnatal day (P)14 (*A*), P21 (*B*), and P34 (*C*).

IC also shows greater genotype difference in response magnitudes at P21, but not P14, suggesting that the cortical hyperresponsivity may be inherited from subcortical sites, including the IC. Similar developmental studies have not been performed in the medial geniculate body.

Consistent with abnormal inhibition, Wen et al. (2018) showed that increased matrix metalloproteinase-9 (MMP-9) in the auditory cortex may lead to abnormal development of perineuronal nets (PNN) and parvalbumin (PV)-positive inhibitory interneurons. Loss of PNNs will reduce excitability of PV cells resulting in reduced network inhibition. This suggests that at least part of the cortical deficit arises due to PV/PNN deficits that are local to cortex and not inherited from the IC. This notion was further supported by a recent study that showed that removal of *Fmr1* only from forebrain excitatory neurons using the *Nex1* promoter results in enhanced low gamma oscillations in the cortex indicating local cortical circuit deficits (Lovelace et al. 2020). Interestingly, however, enhanced high gamma seen in previous cortical recordings from global *Fmr1* KO mice was not present when *Fmr1* was removed only from forebrain neurons. This suggests a combination of cortical and subcortical contributions give rise to the various auditory processing phenotypes studied in the *Fmr1* KO mice. The present study identifies the IC as a potentially strong hub of hypersensitive responses, at least in early development.

Methodological issues. For the c-Fos analysis, up to four mice were exposed together in a cage. Importantly, they were always of the same genotype and age range when tested together. The control (WT) group and the *Fmr1* KO group were tested with identical methods. Therefore, any group testing effects must affect each genotype similarly. However, any differences in social vocalizations or movement related sounds (walking, running, etc.) across genotypes may potentially affect c-Fos expression in auditory nuclei. Future studies will test one mouse at a time, and quantify movement-related sounds to address these caveats.

No counterstaining was used to distinguish layers of the cortex, divisions of the MGB, or the nuclei of the IC. The distinct areas within each auditory region were identified based on mouse brain atlas. Future studies with cytoarchitecture counterstains are needed to identify specific subnuclei with more precision. Electrophysiological responses were recorded under anesthesia, and this may have reduced the spiking activity of individual neurons. Whether the reported hyperactivity of IC neurons in *Fmr1* KO mice may actually be an underestimate remains to be identified with recordings conducted in awake mice.

We did not perform analysis of age-related changes in the density of c-Fos+ cells to identify any differences in developmental trajectories across the genotypes. The reason for this is the use of different sound levels at the two ages studied. We used the loudest sound levels that did not cause AGS at each age tested. The 85- and 90-dB levels used were ~5 dB below AGS threshold at P21 and P34, respectively. However, they were not matched in absolute sound levels.

Conclusions. We found region-specific deficits in both the density of c-Fos+ cells and response properties in the IC of developing *Fmr1* KO mouse. Most of the deficits were seen at P21, the time of high AGS susceptibility. In addition, the main differences were in dorsolateral IC and in neurons tuned to lower frequencies in the IC. This implies that FMRP affects differently low- and high-frequency regions of IC. Future studies should examine AGS with stimuli that are low-pass or high-pass filtered at ~20 kHz to determine if the *Fmr1* KO mice are more sensitive to low-frequency sounds during development. The lack of electrophysiological deficits at P14 indicates abnormal experience-dependent plasticity between P14 and P21, similar to that seen in the auditory cortex (Wen et al. 2018). In addition, studies on the cognitive and social impacts of early life IC dysfunction are needed to address development of autism related behaviors in *Fmr1* KO mice.

It is important to consider that in neurodevelopmental disorders, it is difficult to disambiguate direct effects of genetic changes, the effects of altered experiences of the animal caused by

the genetic change, and the compensatory plasticity mechanisms generated in the brain (Antoine et al. 2019; Bülow et al. 2019). In fact, many phenotypes observed in FXS (human and mice) are only seen transiently or fluctuate during development (Meredith et al. 2012; Vislay et al. 2013; Wen et al. 2019). Even transient disruptions during early development can have long lasting impact. In the case of auditory hypersensitivity in *Fmr1* KO mice, divergence towards hyperresponsiveness appears to occur between P14 and P21. Our data point to the importance of studies to track the developmental trajectories of phenotypes (Razak et al. In press). This will aid in identifying optimal treatment windows during development for clinical trials in FXS.

ACKNOWLEDGMENTS

We thank members of Drs. I. M. Ethell, K. A. Razak, and D. K. Binder laboratories for helpful discussions, comments, and technical support.

GRANTS

This work was supported by the U.S. Army Medical Research Grant W81XWH-15-1-0436.

DISCLOSURES

No conflicts of interest, financial or otherwise, are declared by the authors.

AUTHOR CONTRIBUTIONS

A.O.N., D.K.B., I.M.E., and K.A.R. conceived and designed research; A.O.N. and K.A.R. performed experiments; A.O.N. and K.A.R. analyzed data; A.O.N., D.K.B., I.M.E., and K.A.R. interpreted results of experiments; A.O.N. and K.A.R. prepared figures; A.O.N., D.K.B., I.M.E., and K.A.R. drafted manuscript; A.O.N., D.K.B., I.M.E., and K.A.R. edited and revised manuscript; A.O.N., D.K.B., I.M.E., and K.A.R. approved final version of manuscript.

REFERENCES

Aitkin LM, Moore DR. Inferior colliculus. II. Development of tuning characteristics and tonotopic organization in central nucleus of the neonatal cat. *J Neurophysiol* 38: 1208–1216, 1975. doi:10.1152/jn.1975.38.5.1208.

Antoine MW, Langberg T, Schnepel P, Feldman DE. Increased excitation-inhibition ratio stabilizes synapse and circuit excitability in four autism mouse models. *Neuron* 101: 648–661.e4, 2019. doi:10.1016/j.neuron.2018.12.026.

Arnault P, Roger M. The connections of the peripeduncular area studied by retrograde and anterograde transport in the rat. *J Comp Neurol* 258: 463–476, 1987. doi:10.1002/cne.902580313.

Bakker CE, Oostra BA. Understanding fragile X syndrome: insights from animal models. *Cytogenet Genome Res* 100: 111–123, 2003. doi:10.1159/000072845.

Beebe K, Wang Y, Kulesza R. Distribution of fragile X mental retardation protein in the human auditory brainstem. *Neuroscience* 273: 79–91, 2014. doi:10.1016/j.neuroscience.2014.05.006.

Brown MR, Kronengold J, Gazula V-R, Chen Y, Strumbos JG, Sigworth FJ, Navaratnam D, Kaczmarek LK. Fragile X mental retardation protein controls gating of the sodium-activated potassium channel Slack. *Nat Neurosci* 13: 819–821, 2010. doi:10.1038/nn.2563.

Bülow P, Murphy TJ, Bassell GJ, Wenner P. Homeostatic intrinsic plasticity is functionally altered in Fmr1 KO cortical neurons. *Cell Reports* 26: 1378–1388.e3, 2019. doi:10.1016/j.celrep.2019.01.035.

Castrén M, Pääkkönen A, Tarkka IM, Ryynänen M, Partanen J. Augmentation of auditory N1 in children with fragile X syndrome. *Brain Topogr* 15: 165–171, 2003. doi:10.1023/A:1022606200636.

Chen L, Toth M. Fragile X mice develop sensory hyperreactivity to auditory stimuli. *Neuroscience* 103: 1043–1050, 2001. doi:10.1016/S0306-4522(01)00036-7.

Cho JH, Bayazitov IT, Meloni EG, Myers KM, Carlezon WA Jr, Zakharenko SS, Bolshakov VY. Coactivation of thalamic and cortical pathways induces input timing-dependent plasticity in amygdala. *Nat Neurosci* 15: 113–122, 2011. doi:10.1038/nn.2993.

Choy Buentello D, Bishop DC, Oliver DL. Differential distribution of GABA and glycine terminals in the inferior colliculus of rat and mouse. *J Comp Neurol* 523: 2683–2697, 2015. doi:10.1002/cne.23810.

Cramer KS, Gabriele ML. Axon guidance in the auditory system: multiple functions of Eph receptors. *Neuroscience* 277: 152–162, 2014. doi:10.1016/j.neuroscience.2014.06.068.

Curia G, Papouin T, Séguéla P, Avoli M. Downregulation of tonic GABAergic inhibition in a mouse model of fragile X syndrome. *Cereb Cortex* 19: 1515–1520, 2009. doi:10.1093/cercor/bhn159.

D'Hulst C, De Geest N, Reeve SP, Van Dam D, De Deyn PP, Hassan BA, Kooy RF. Decreased expression of the GABAA receptor in fragile X syndrome. *Brain Res* 1121: 238–245, 2006. doi:10.1016/j.brainres.2006.08.115.

Dansie LE, Phommahaxay K, Okusanya AG, Uwadia J, Huang M, Rotschafer SE, Razak KA, Ethell DW, Ethell IM. Long-lasting effects of minocycline on behavior in young but not adult Fragile X mice. *Neuroscience* 246: 186–198, 2013. doi:10.1016/j.neuroscience.2013.04.058.

Dölen G, Osterweil E, Rao BS, Smith GB, Auerbach BD, Chattarji S, Bear MF. Correction of fragile X syndrome in mice. *Neuron* 56: 955–962, 2007. doi:10.1016/j.neuron.2007.12.001.

Ehret G, Romand R. Development of tone response thresholds, latencies and tuning in the mouse inferior colliculus. *Brain Res Dev Brain Res* 67: 317–326, 1992. doi:10.1016/0165-3806(92)90233-M.

Ethridge LE, White SP, Mosconi MW, Wang J, Byerly MJ, Sweeney JA. Reduced habituation of auditory evoked potentials indicate cortical hyper-excitability in Fragile X Syndrome. *Transl Psychiatry* 6: e787, 2016. doi:10.1038/tp.2016.48.

Ethridge LE, White SP, Mosconi MW, Wang J, Pedapati EV, Erickson CA, Byerly MJ, Sweeney JA. Neural synchronization deficits linked to cortical hyper-excitability and auditory hypersensitivity in fragile X syndrome. *Mol Autism* 8: 22, 2017 [Erratum in *Mol Autism* 8: 38, 2017]. doi:10.1186/s13229-017-0140-1.

Faingold CL. Role of GABA abnormalities in the inferior colliculus pathophysiology—audiogenic seizures. *Hear Res* 168: 223–237, 2002. doi:10.1016/S0378-5955(02)00373-8.

Faingold CL, Anderson CA. Loss of intensity-induced inhibition in inferior colliculus neurons leads to audiogenic seizure susceptibility in behaving genetically epilepsy-prone rats. *Exp Neurol* 113: 354–363, 1991. doi:10.1016/0014-4886(91)90026-9.

Faingold CL, Boersma Anderson CA, Caspary DM. Involvement of GABA in acoustically-evoked inhibition in inferior colliculus neurons. *Hear Res* 52: 201–216, 1991. doi:10.1016/0378-5955(91)90200-S.

Faingold CL, Randall ME. Neurons in the deep layers of superior colliculus play a critical role in the neuronal network for audiogenic seizures: mechanisms for production of wild running behavior. *Brain Res* 815: 250–258, 1999. doi:10.1016/S0006-8993(98)01136-6.

Fathke RL, Gabriele ML. Patterning of multiple layered projections to the auditory midbrain prior to experience. *Hear Res* 249: 36–43, 2009. doi:10.1016/j.heares.2009.01.004.

Felix RA II, Portfors CV. Excitatory, inhibitory and facilitatory frequency response areas in the inferior colliculus of hearing impaired mice. *Hear Res* 228: 212–229, 2007. doi:10.1016/j.heares.2007.02.009.

Frankland PW, Wang Y, Rosner B, Shimizu T, Balleine BW, Dykens EM, Ornitz EM, Silva AJ. Sensorimotor gating abnormalities in young males with fragile X syndrome and Fmr1-knockout mice. *Mol Psychiatry* 9: 417–425, 2004. doi:10.1038/sj.mp.4001432.

Fulop DB, Humli V, Szepesy J, Ott V, Reglodi D, Gaszner B, Nemeth A, Szirmai A, Tamas L, Hashimoto H, Zelles T, Tamas A. Hearing impairment and associated morphological changes in pituitary adenylate cyclase activating polypeptide (PACAP)-deficient mice. *Sci Rep* 9: 14598, 2019. doi:10.1038/s41598-019-50775-z.

Fuzessery ZM, Hall JC. Role of GABA in shaping frequency tuning and creating FM sweep selectivity in the inferior colliculus. *J Neurophysiol* 76: 1059–1073, 1996. doi:10.1152/jn.1996.76.2.1059.

Gabriele ML, Brunso-Bechtold JK, Henkel CK. Plasticity in the development of afferent patterns in the inferior colliculus of the rat after unilateral cochlear ablation. *J Neurosci* 20: 6939–6949, 2000a. doi:10.1523/JNEUROSCI.20-18-06939.2000.

Gabriele ML, Brunso-Bechtold JK, Henkel CK. Development of afferent patterns in the inferior colliculus of the rat: projection from the dorsal nucleus of the lateral lemniscus. *J Comp Neurol* 416: 368–382, 2000b. doi:10.1002/(SICI)1096-9861(20000117)416:3<368:AID-CNE8>3.0.CO;2-C.

Garcia-Pino E, Gessele N, Koch U. Enhanced excitatory connectivity and disturbed sound processing in the auditory brainstem of fragile X mice. *J Neurosci* 37: 7403–7419, 2017. doi:10.1523/JNEUROSCI.2310-16.2017.

Goldberg JM, Brown PB. Response of binaural neurons of dog superior olivary complex to dichotic tonal stimuli: some physiological mechanisms of sound localization. *J Neurophysiol* 32: 613–636, 1969. doi:10.1152/jn.1969.32.4.613.

Gonzalez D, Tomasek M, Hays S, Sridhar V, Ammanuel S, Chang CW, Pawlowski K, Huber KM, Gibson JR. Audiogenic seizures in the *Fmr1* knock-out mouse are induced by *Fmr1* deletion in subcortical, VGlut2-expressing excitatory neurons and require deletion in the inferior colliculus. *J Neurosci* 39: 9852–9863, 2019. doi:10.1523/JNEUROSCI.0886-19.2019.

Grimsley CA, Sanchez JT, Sivaramakrishnan S. Midbrain local circuits shape sound intensity codes. *Front Neural Circuits* 7: 174, 2013. doi:10.3389/fncir.2013.00174.

Henkel CK, Keiger CJ, Franklin SR, Brunso-Bechtold JK. Development of banded afferent compartments in the inferior colliculus before onset of hearing in ferrets. *Neuroscience* 146: 225–235, 2007. doi:10.1016/j.neuroscience.2007.01.016.

Hitoglou M, Ververi A, Antoniadis A, Zafeiriou DI. Childhood autism and auditory system abnormalities. *Pediatr Neurol* 42: 309–314, 2010. doi:10.1016/j.pediatrneurol.2009.10.009.

Howorth PW, Teschemacher AG, Pickering AE. Retrograde adenoviral vector targeting of nociresponsive pontospinal noradrenergic neurons in the rat in vivo. *J Comp Neurol* 512: 141–157, 2009. doi:10.1002/cne.21879.

Hurley LM, Tracy JA, Bohorquez A. Serotonin 1B receptor modulates frequency response curves and spectral integration in the inferior colliculus by reducing GABAergic inhibition. *J Neurophysiol* 100: 1656–1667, 2008. doi:10.1152/jn.90536.2008.

Kazdoba TM, Leach PT, Silverman JL, Crawley JN. Modeling fragile X syndrome in the Fmr1 knockout mouse. *Intractable Rare Dis Res* 3: 118–133, 2014. doi:10.5582/irdr.2014.01024.

Kokash J, Alderson EM, Reinhard SM, Crawford CA, Binder DK, Ethell IM, Razak KA. Genetic reduction of MMP-9 in the Fmr1 KO mouse partially rescues prepulse inhibition of acoustic startle response. *Brain Res* 1719: 24–29, 2019. doi:10.1016/j.brainres.2019.05.029.

Kulinich AO, Reinhard SM, Rais M, Lovelace JW, Scott V, Binder DK, Razak KA, Ethell IM. Beneficial effects of sound exposure on auditory cortex development in a mouse model of Fragile X Syndrome. *Neurobiol Dis* 134: 104622, 2020. doi:10.1016/j.nbd.2019.104622.

Le Beau FE, Rees A, Malmierca MS. Contribution of GABA- and glycine-mediated inhibition to the monaural temporal response properties of neurons in the inferior colliculus. *J Neurophysiol* 75: 902–919, 1996. doi:10.1152/jn.1996.75.2.902.

LeDoux JE, Farb CR, Milner TA. Ultrastructure and synaptic associations of auditory thalamo-amygdala projections in the rat. *Exp Brain Res* 85: 577–586, 1991. doi:10.1007/BF00231742.

Lovelace JW, Ethell IM, Binder DK, Razak KA. Translation-relevant EEG phenotypes in a mouse model of Fragile X Syndrome. *Neurobiol Dis* 115: 39–48, 2018. doi:10.1016/j.nbd.2018.03.012.

Lovelace JW, Rais M, Palacios AR, Shuai XS, Bishay S, Popa O, Pirbhoy PS, Binder DK, Nelson DL, Ethell IM, Razak KA. Deletion of Fmr1 from forebrain excitatory neurons triggers abnormal cellular, EEG, and behavioral phenotypes in the auditory cortex of a mouse model of Fragile X Syndrome. *Cereb Cortex* 30: 969–988, 2020. doi:10.1093/cercor/bhz141.

Lovelace JW, Wen TH, Reinhard S, Hsu MS, Sidhu H, Ethell IM, Binder DK, Razak KA. Matrix metalloproteinase-9 deletion rescues auditory evoked potential habituation deficit in a mouse model of fragile X syndrome. *Neurobiol Dis* 89: 126–135, 2016. doi:10.1016/j.nbd.2016.02.002.

Martin del Campo HN, Measor KR, Razak KA. Parvalbumin immunoreactivity in the auditory cortex of a mouse model of presbycusis. *Hear Res* 294: 31–39, 2012. doi:10.1016/j.heares.2012.08.017.

McCullagh EA, Rotschafer SE, Auerbach BD, Klug A, Kaczmarek LK, Cramer KS, Kulesza RJ Jr, Razak KA, Lovelace JW, Lu Y, Koch U, Wang Y. Mechanisms underlying auditory processing deficits in fragile X syndrome. *FASEB J* 34: 3501–3518, 2020. doi:10.1096/fj.201902435R.

Merchán M, Aguilar LA, Lopez-Poveda EA, Malmierca MS. The inferior colliculus of the rat: quantitative immunocytochemical study of GABA and glycine. *Neuroscience* 136: 907–925, 2005. doi:10.1016/j.neuroscience.2004.12.030.

Meredith RM, Dawitz J, Kramvis I. Sensitive time-windows for susceptibility in neurodevelopmental disorders. *Trends Neurosci* 35: 335–344, 2012. doi:10.1016/j.tins.2012.03.005.

Michalon A, Sidorov M, Ballard TM, Ozmen L, Spooren W, Wettstein JG, Jaeschke G, Bear MF, Lindemann L. Chronic pharmacological mGlu5 inhibition corrects fragile X in adult mice. *Neuron* 74: 49–56, 2012. doi:10.1016/j.neuron.2012.03.009.

Millan MH, Meldrum BS, Faingold CL. Induction of audiogenic seizure susceptibility by focal infusion of excitant amino acid or bicuculline into the inferior colliculus of normal rats. *Exp Neurol* 91: 634–639, 1986. doi:10.1016/0014-4886(86)90059-2.

Miller LJ, McIntosh DN, McGrath J, Shyu V, Lampe M, Taylor AK, Tassone F, Neitzel K, Stackhouse T, Hagerman RJ. Electrodermal responses to sensory stimuli in individuals with fragile X syndrome: a preliminary report. *Am J Med Genet* 83: 268–279, 1999. doi:10.1002/(SICI)1096-8628(19990402)83:4<268:AID-AJMG7>3.0.CO;2-K.

Musumeci SA, Bosco P, Calabrese G, Bakker C, De Sarro GB, Elia M, Ferri R, Oostra BA. Audiogenic seizures susceptibility in transgenic mice with fragile X syndrome. *Epilepsia* 41: 19–23, 2000. doi:10.1111/j.1528-1157.2000.tb01499.x.

Musumeci SA, Calabrese G, Bonaccorso CM, D'Antoni S, Brouwer JR, Bakker CE, Elia M, Ferri R, Nelson DL, Oostra BA, Catania MV. Audiogenic seizure susceptibility is reduced in fragile X knockout mice after introduction of FMR1 transgenes. *Exp Neurol* 203: 233–240, 2007. doi:10.1016/j.expneurol.2006.08.007.

Numa C, Nagai H, Taniguchi M, Nagai M, Shinohara R, Furuyashiki T. Social defeat stress-specific increase in c-Fos expression in the extended amygdala in mice: Involvement of dopamine D1 receptor in the medial prefrontal cortex. *Sci Rep* 9: 16670, 2019. doi:10.1038/s41598-019-52997-7.

Oswald AM, Reyes AD. Maturation of intrinsic and synaptic properties of layer 2/3 pyramidal neurons in mouse auditory cortex. *J Neurophysiol* 99: 2998–3008, 2008. doi:10.1152/jn.01160.2007.

Oswald AM, Reyes AD. Development of inhibitory timescales in auditory cortex. *Cereb Cortex* 21: 1351–1361, 2011. doi:10.1093/cercor/bhq214.

Pacey LK, Heximer SP, Hampson DR. Increased GABA(B) receptor-mediated signaling reduces the susceptibility of fragile X knockout mice to audiogenic seizures. *Mol Pharmacol* 76: 18–24, 2009. doi:10.1124/mol.109.056127.

Palombi PS, Caspary DM. GABA inputs control discharge rate primarily within frequency receptive fields of inferior colliculus neurons. *J Neurophysiol* 75: 2211–2219, 1996. doi:10.1152/jn.1996.75.6.2211.

Phillips DP, Kelly JB. Coding of tone-pulse amplitude by single neurons in auditory cortex of albino rats (Rattus norvegicus). *Hear Res* 37: 269–279, 1989. doi:10.1016/0378-5955(89)90027-0.

Preibisch S, Saalfeld S, Tomancak P. Globally optimal stitching of tiled 3D microscopic image acquisitions. *Bioinformatics* 25: 1463–1465, 2009. doi:10.1093/bioinformatics/btp184.

Rais M, Binder DK, Razak KA, Ethell IM. Sensory processing phenotypes in fragile X syndrome. *ASN Neuro* 10: 1759091418801092, 2018. doi:10.1177/1759091418801092.

Razak KA, Dominick K, Erickson CA. Developmental studies in fragile X syndrome. *J Neurodev Disord* 12: 13, 2020. doi:10.1186/s11689-020-09310-9.

Reinhard SM, Rais M, Afroz S, Hanania Y, Pendi K, Espinoza K, Rosenthal R, Binder DK, Ethell IM, Razak KA. Reduced perineuronal net expression in Fmr1 KO mice auditory cortex and amygdala is linked to impaired fear-associated memory. *Neurobiol Learn Mem* 164: 107042, 2019. doi:10.1016/j.nlm.2019.107042.

Rogers SJ, Hepburn S, Wehner E. Parent reports of sensory symptoms in toddlers with autism and those with other developmental disorders. *J Autism Dev Disord* 33: 631–642, 2003. doi:10.1023/B:JADD.0000006000.38991.a7.

Romand R, Ehret G. Development of tonotopy in the inferior colliculus. I. Electrophysiological mapping in house mice. *Brain Res Dev Brain Res* 54: 221–234, 1990. doi:10.1016/0165-3806(90)90145-O.

Rotschafer S, Razak K. Altered auditory processing in a mouse model of fragile X syndrome. *Brain Res* 1506: 12–24, 2013. doi:10.1016/j.brainres.2013.02.038.

Rotschafer SE, Cramer KS. Developmental emergence of phenotypes in the auditory brainstem nuclei of Fmr1 knockout mice. *eNeuro* 4: ENEURO.0264-17.2017, 2017. doi:10.1523/ENEURO.0264-17.2017

Rotschafer SE, Marshak S, Cramer KS. Deletion of Fmr1 alters function and synaptic inputs in the auditory brainstem. *PLoS One* 10: e0117266, 2015. doi:10.1371/journal.pone.0117266.

Ruby K, Falvey K, Kulesza RJ. Abnormal neuronal morphology and neurochemistry in the auditory brainstem of Fmr1 knockout rats. *Neuroscience* 303: 285–298, 2015. doi:10.1016/j.neuroscience.2015.06.061.

Sanes DH, Geary WA, Wooten GF, Rubel EW. Quantitative distribution of the glycine receptor in the auditory brain stem of the gerbil. *J Neurosci* 7: 3793–3802, 1987. doi:10.1523/JNEUROSCI.07-11-03793.1987.

Schneider A, Leigh MJ, Adams P, Nanakul R, Chechi T, Olichney J, Hagerman R, Hessl D. Electrocortical changes associated with minocycline treatment in fragile X syndrome. *J Psychopharmacol* 27: 956–963, 2013. doi:10.1177/0269881113494105.

Shnerson A, Willott JF. Development of inferior colliculus response properties in C57BL/6J mouse pups. *Exp Brain Res* 37: 373–385, 1979. doi:10.1007/BF00237720.

Smith LE, Barker ET, Seltzer MM, Abbeduto L, Greenberg JS. Behavioral phenotype of fragile X syndrome in adolescence and adulthood. *Am J Intellect Dev Disabil* 117: 1–17, 2012. doi:10.1352/1944-7558-117.1.1.

Strumbos JG, Brown MR, Kronengold J, Polley DB, Kaczmarek LK. Fragile X mental retardation protein is required for rapid experience-dependent regulation of the potassium channel Kv3.1b. *J Neurosci* 30: 10263–10271, 2010. doi:10.1523/JNEUROSCI.1125-10.2010.

Sturm J, Nguyen T, Kandler K. Development of intrinsic connectivity in the central nucleus of the mouse inferior colliculus. *J Neurosci* 34: 15032–15046, 2014. doi:10.1523/JNEUROSCI.2276-14.2014.

Vislay RL, Martin BS, Olmos-Serrano JL, Kratovac S, Nelson DL, Corbin JG, Huntsman MM. Homeostatic responses fail to correct defective amygdala inhibitory circuit maturation in fragile X syndrome. *J Neurosci* 33: 7548–7558, 2013. doi:10.1523/JNEUROSCI.2764-12.2013.

Wang J, Ethridge LE, Mosconi MW, White SP, Binder DK, Pedapati EV, Erickson CA, Byerly MJ, Sweeney JA. A resting EEG study of neocortical hyperexcitability and altered functional connectivity in fragile X syndrome. *J Neurodev Disord* 9: 11, 2017. doi:10.1186/s11689-017-9191-z.

Wang Y, Sakano H, Beebe K, Brown MR, de Laat R, Bothwell M, Kulesza RJ Jr, Rubel EW. Intense and specialized dendritic localization of the fragile X mental retardation protein in binaural brainstem neurons: a comparative study in the alligator, chicken, gerbil, and human. *J Comp Neurol* 522: 2107–2128, 2014. doi:10.1002/cne.23520.

Wen TH, Afroz S, Reinhard SM, Palacios AR, Tapia K, Binder DK, Razak KA, Ethell IM. Genetic reduction of matrix metalloproteinase-9 promotes formation of perineuronal nets around parvalbumin-expressing interneurons and normalizes auditory cortex responses in developing Fmr1 knock-out mice. *Cereb Cortex* 28: 3951–3964, 2018. doi:10.1093/cercor/bhx258.

Wen TH, Lovelace JW, Ethell IM, Binder DK, Razak KA. Developmental changes in EEG phenotypes in a mouse model of fragile X syndrome. *Neuroscience* 398: 126–143, 2019. doi:10.1016/j.neuroscience.2018.11.047.

Yan QJ, Rammal M, Tranfaglia M, Bauchwitz RP. Suppression of two major Fragile X Syndrome mouse model phenotypes by the mGluR5 antagonist MPEP. *Neuropharmacology* 49: 1053–1066, 2005. doi:10.1016/j.neuropharm.2005.06.004.

Yang Y, Lee J, Kim G. Integration of locomotion and auditory signals in the mouse inferior colliculus. *eLife* 9: e52228, 2020. doi:10.7554/eLife.52228.

Zhang H, Kelly JB. Glutamatergic and GABAergic regulation of neural responses in inferior colliculus to amplitude-modulated sounds. *J Neurophysiol* 90: 477–490, 2003. doi:10.1152/jn.01084.2002.